



Amplitude analysis of $B^0 \rightarrow \eta_c(1S)K^+\pi^-$ decays

LHCb Collaboration*

European Organization for Nuclear Research (CERN), Geneva, Switzerland

Received: 4 September 2025 / Accepted: 21 February 2026
© CERN for the benefit of the LHCb collaboration 2026

Abstract An amplitude analysis of the $B^0 \rightarrow \eta_c(1S)K^+\pi^-$ decays with $\eta_c(1S) \rightarrow p\bar{p}$ is performed using a sample corresponding to an integrated luminosity of 9 fb^{-1} of pp collision data collected by the LHCb detector at centre-of-mass energies of $\sqrt{s} = 7, 8$ and 13 TeV . The data are described with a model including only intermediate contributions from known K^{*0} resonances. Evidence for an exotic resonance in the $\eta_c(1S)\pi^-$ system, reported in a previous analysis of this decay channel, is not confirmed. The inclusive branching fraction of the $B^0 \rightarrow \eta_c(1S)K^+\pi^-$ decays is measured to be

$$\mathcal{B}(B^0 \rightarrow \eta_c(1S)K^+\pi^-) = (5.82 \pm 0.20 \pm 0.23 \pm 0.55) \times 10^{-4},$$

where the first uncertainty is statistical, the second systematic, and the third arises from the limited knowledge of external branching fractions.

1 Introduction

Since the formulation of the quark model, hadronic states beyond the conventional $q\bar{q}$ mesons and qqq baryons have been proposed. Models based on quantum chromodynamics predict the existence of various nonconventional hadrons, composed of different combinations of quarks and gluons, including glueballs, molecular states and tightly bound states, such as pentaquarks ($qqqq\bar{q}$) and tetraquarks ($qq\bar{q}\bar{q}$) [1, 2]. In the early 2000s, a hadron with unexpected properties, the $\chi_{c1}(3872)$ meson, was observed [3], followed shortly by the discovery of many other charmonium-like and bottomonium-like states [4–7]. In some cases the properties of these states, including their electric charge, are inconsistent with predictions from conventional $q\bar{q}$ models. Various interpretations have been proposed regarding their nature, binding and production mechanisms, and internal structure [8–13]. To

advance the understanding of these exotic hadrons, it is essential to investigate alternative production mechanisms and decay modes of previously observed unconventional states, while also searching for new candidates.

The BESIII collaboration observed in the $J/\psi\pi^+\pi^-$ final state a resonance whose minimal composition requires the presence of two quarks and two antiquarks [14], denoted $T_{c\bar{c}1}(3900)^-$, later confirmed also by the Belle [15] and CLEO collaborations [16]. This state has been interpreted as a hadrocharmonium state with J/ψ embedded in excited light-quark matter [17], implying a partner state where the J/ψ is replaced by the $\eta_c(1S)$. Such a state would correspond to an isovector resonance decaying to $\eta_c(1S)\pi^-$ with similar structure and quantum numbers.¹ This interpretation is further supported by heavy-quark spin symmetry [17], lattice QCD [18], and diquark models [9], which all foresee such a decay channel.

Evidence of a state decaying to $\eta_c\pi^-$, named $T_{c\bar{c}}(4100)^-$, has been found in the previous Dalitz Plot (DP) [19] analysis of $B^0 \rightarrow \eta_c K^+\pi^-$ decays by the LHCb collaboration [20] using a data sample of pp collisions corresponding to an integrated luminosity of 4.7 fb^{-1} , collected in 2011, 2012 and 2016 at centre-of-mass energies of $\sqrt{s} = 7, 8$, and 13 TeV , respectively.² The mass and natural width of this resonance are measured to be $4096 \pm 20_{-22}^{+18} \text{ MeV}$ and $152 \pm 58_{-35}^{+60} \text{ MeV}$, respectively.³ Since this would make the state significantly more massive than the $T_{c\bar{c}1}(3900)^-$ state, it cannot be its expected partner. Following the evidence reported by the LHCb collaboration for the $T_{c\bar{c}}(4100)^-$ charmonium-like candidate, several theoretical studies have been conducted to investigate its nature. The authors of Ref. [21] calculated the mass, width, and coupling of this resonance, treating it as a scalar four-quark system with a diquark-antidiquark struc-

* e-mail: gabriele.romolini@cern.ch

¹ The simplified notation η_c is used to refer to the $\eta_c(1S)$ meson.

² The inclusion of charge-conjugate processes is implied throughout.

³ Natural units with $\hbar = c = 1$ are used throughout.

ture. Other studies found the $T_{c\bar{c}}(4100)^-$ state to be compatible with the tetraquark hypothesis favouring the quantum number $J^{PC} = 0^{++}$ based on the measured width [22]. The study reported in Ref. [23] suggests that the state can be described as hadrocharmonium, where the η_c charmonium core is embedded in an S-wave configuration inside an excited light-quark state with the quantum numbers of a pion, $I^G(J^P) = 1^-(0^-)$. It further proposes that the mass difference between the $T_{c\bar{c}}(4200)^-$, observed in the $J/\psi K^+\pi^-$ final state [24,25], and $T_{c\bar{c}}(4100)^-$ states should be similar to that between the J/ψ and η_c mesons, and that the partial widths of their dominant decays to $J/\psi\pi^-$ and $\eta_c\pi^-$, respectively, should be the same. There are also studies [26] proposing that $T_{c\bar{c}}(4100)^-$ is the charge-conjugate state of the $T_{c\bar{c}}(4050)^+$ state observed by the Belle collaboration in the $\chi_{c1}\pi^+$ final state [27]. Finally, it has been suggested that the observed structure could be a kinematic effect arising from an S-wave $D^*\bar{D}^*$ pair rescattering with $I^G(J^{PC}) = 1^-(0^{++})$ or a resonance produced by the P-wave $D^*\bar{D}^*$ interaction [28].

This letter reports an updated study of the $B^0 \rightarrow \eta_c K^+\pi^-$ decay with a dataset approximately twice the size of the one used in Ref. [20] which enables a more precise evaluation of the presence of exotic contributions in this decay, as well as a more accurate determination of their properties. The $B^0 \rightarrow \eta_c K^+\pi^-$ decay is expected to be dominated by the $K^{*0}(892) \rightarrow K^+\pi^-$ resonance, with some contributions from other $K^{*0} \rightarrow K^+\pi^-$ resonances. The decay could also proceed through exotic intermediate states, which could result in resonant structures in the $\eta_c\pi^-$ system. The Feynman diagrams of the $B^0 \rightarrow \eta_c K^+\pi^-$ decay are shown in Fig. 1. The $B^0 \rightarrow \eta_c K^+\pi^-$ decay is studied by reconstructing the η_c meson through its $p\bar{p}$ decay mode rather than the dominant mesonic modes. This choice avoids the need to distinguish between kaons and pions originating from B^0 decay, reducing associated systematic uncertainties [29]. The $B^0 \rightarrow \eta_c K^+\pi^-$ decay involves only pseudoscalar mesons in the initial and final states and it is therefore fully described by two independent kinematic variables. This allows for a DP analysis, which provides a complete characterisation of the decay dynamics in the assumption of no sizeable effects due to additional interfering amplitudes, involving suppressed Flavour Changing Neutral Currents, with the same $B^0 \rightarrow p\bar{p}K^+\pi^-$ final state.

The absolute branching fraction of the $B^0 \rightarrow \eta_c K^+\pi^-$ decay is also measured, using the $B^0 \rightarrow J/\psi K^+\pi^-$ decay as normalisation channel. The data sample corresponds to an integrated luminosity of 9 fb^{-1} of pp collision data collected by the LHCb detector at centre-of-mass energies of $\sqrt{s} = 7, 8, \text{ and } 13 \text{ TeV}$ in 2011, 2012 and 2015–2018, respectively. Data collected in 2011 and 2012 are referred to as Run 1 data, while data collected in 2015–2018 are referred to as Run 2 data.

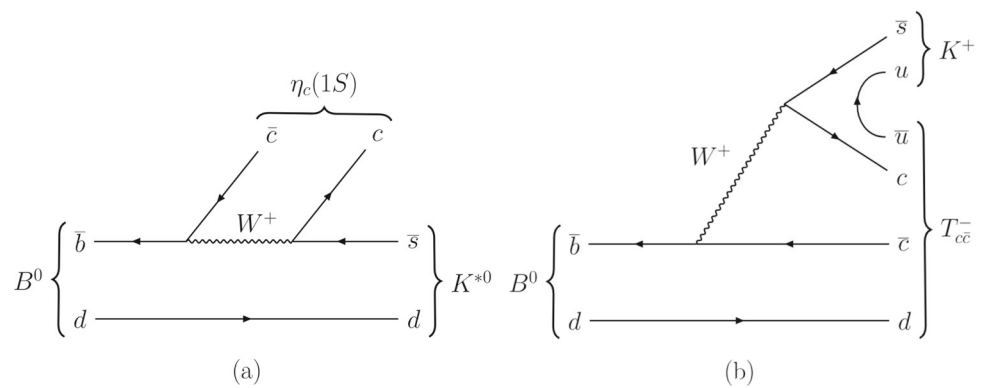
2 Detector and simulation

The LHCb detector [30,31] is a single-arm forward spectrometer covering the pseudorapidity range $2 < \eta < 5$, designed for the study of particles containing b or c quarks. The detector used to collect the data analysed in this paper includes a high-precision tracking system consisting of a silicon-strip vertex detector surrounding the pp interaction region [32], a large-area silicon-strip detector located upstream of a dipole magnet with a bending power of about 4 T m, and three stations of silicon-strip detectors and straw drift tubes [33,34] placed downstream of the magnet. The tracking system provides a measurement of the momentum, p , of charged particles with a relative uncertainty that varies from 0.5% at low momentum to 1.0% at 200 GeV. The minimum distance of a track to a primary pp collision vertex (PV), the impact parameter (IP), is measured with a resolution of $(15 + 29/p_T) \mu\text{m}$, where p_T is the component of the momentum transverse to the beam, in GeV. Different types of charged hadrons are distinguished using information from two ring-imaging Cherenkov detectors [35]. Photons, electrons, and hadrons are identified by a calorimeter system consisting of scintillating-pad and preshower detectors, an electromagnetic and a hadronic calorimeter. Muons are identified by a system composed of alternating layers of iron and multiwire proportional chambers [36]. The online event selection is performed by a trigger system [37], which consists of a hardware stage, based on information from the calorimeter and muon systems, followed by a software stage, which applies a full event reconstruction.

At the hardware trigger stage, events are required to have a muon with high p_T or a hadron, photon or electron with high transverse energy in the calorimeters. For hadrons, the transverse energy threshold is 3.5 GeV. The software trigger requires a two-, three- or four-track secondary vertex with a significant displacement from any primary pp interaction vertex. At least one charged particle must have a transverse momentum $p_T > 1.6 \text{ GeV}$ and be inconsistent with originating from any PV. A multivariate algorithm [38,39] is used for the identification of secondary vertices consistent with the decay of a b hadron.

Simulated events are used to develop the selection requirements, validate fit models, and to evaluate the efficiencies needed for the inclusive branching fraction measurement and the amplitude analysis. In the simulation, pp collisions are generated using PYTHIA [40] with a specific LHCb configuration [41]. Decays of unstable particles are described by EVTGEN [42], in which final-state radiation is generated using PHOTOS [43]. The interaction of the generated particles with the detector, and its response, are implemented using the GEANT4 toolkit [44,45] as described in Ref. [46]. The underlying pp interaction is reused multiple times, each with an independently generated signal decay [47].

Fig. 1 Feynman diagrams for the **a** $B^0 \rightarrow \eta_c(1S)K^{*0}$ and **b** $B^0 \rightarrow T_{c\bar{c}}(4100)^- K^+$ decay modes



3 Selection of $B^0 \rightarrow p\bar{p}K^+\pi^-$ candidates

Candidate B^0 mesons are reconstructed in the $B^0 \rightarrow p\bar{p}K^+\pi^-$ decay over the full $m_{p\bar{p}}$ range. The signal channel $B^0 \rightarrow \eta_c K^+\pi^-$ and the normalisation channel $B^0 \rightarrow J/\psi K^+\pi^-$ are obtained by requiring $m_{p\bar{p}}$ to lie within their respective charmonium-resonance regions, 2908–3058 MeV for the η_c meson and 3072–3122 MeV for the J/ψ meson. An initial offline selection is applied to reconstructed particles. Final-state particles are required to have $p_T > 300$ MeV, be inconsistent with originating from any PV, lie within the acceptance of the RICH detectors ($2.0 < \eta < 4.9$) and be compatible with the appropriate proton, kaon or pion mass hypotheses. Furthermore, proton candidates are required to have $10 < p < 150$ GeV, while pion and kaon candidates must have $3 < p < 150$ GeV. Candidate B^0 mesons are required to have a small χ^2_{IP} with respect to a PV, where χ^2_{IP} is defined as the change in the vertex-fit χ^2 of a given PV when reconstructed with and without including the candidate under consideration. The PV providing the smallest χ^2_{IP} value is associated to the B^0 candidate, which is also required to be consistent with originating from this PV by applying a criterion on the angle between its momentum vector and the displacement vector from the PV to its decay vertex. To enhance the resolution of kinematic quantities, such as the diproton mass distribution $m_{p\bar{p}}$ and the two-particle mass combinations that define the DP, a kinematic fit is performed [48]. In this fit, the B^0 candidate is constrained to originate from its associated PV, and its reconstructed mass is constrained to the known B^0 mass [49].

A boosted decision tree (BDT) algorithm [50,51] is used to suppress combinatorial background, corresponding to B^0 candidates formed by uncorrelated particles. Simulated samples of $B^0 \rightarrow p\bar{p}K^+\pi^-$ decays, generated uniformly within the available phase space of the decay, are taken as a signal proxy. The data in the mass $m_{p\bar{p}K^+\pi^-}$ region 5450–5550 MeV is used as a background proxy when training the BDT, to avoid regions containing partially reconstructed b -hadron decays. Two BDT classifiers are trained separately for

Run 1 and Run 2, in order to take into account differences between the two data-taking periods.

The input variables to the BDT classifiers are: the vertex-fit χ^2 , χ^2_{IP} , a discriminating variable evaluating the pointing consistency of the reconstructed B^0 momentum to the B^0 decay vertex, the flight-distance significance of the reconstructed B^0 candidates; the maximum distance of closest approach between final-state particles, and the maximum and minimum p and p_T of the proton and antiproton. The Run 2 BDT additionally uses particle-identification variables of the final-state particles. These variables are adjusted to match the calibration data distributions and are not included in the Run 1 BDT due to the lack of suitable calibration samples [52,53]. The selection criteria on the BDT output are chosen in order to maximise the figure of merit defined as $S/\sqrt{S+B}$, where S is the observed $B^0 \rightarrow p\bar{p}K^+\pi^-$ signal yield before any BDT selection multiplied by the efficiency of the BDT requirement evaluated using simulation, while B is the combinatorial background yield, both obtained in the $m_{p\bar{p}K^+\pi^-}$ region 5200–5360 MeV. Finally, the $\bar{D}^0 \rightarrow K^+\pi^-$, $\bar{\Lambda}_c^- \rightarrow \bar{p}K^+\pi^-$, and $\phi \rightarrow K^+K^-$ decays are vetoed by excluding the mass ranges 1835–1880 MeV, 2250–2305 MeV, and 1010–1028 MeV in the $m_{K^+\pi^-}$, $m_{\bar{p}K^+\pi^-}$, and $m_{K^+K^-}$ distributions, respectively, where the $m_{K^+K^-}$ mass has been reconstructed assigning the K^- meson mass to the π^- candidate.

3.1 Signal yield of $B^0 \rightarrow \eta_c K^+\pi^-$ decay

Prior to the DP fit, a two-dimensional extended maximum-likelihood fit to the $m_{p\bar{p}K^+\pi^-}$ and $m_{p\bar{p}}$ mass distributions is performed in order to isolate the $B^0 \rightarrow \eta_c(\rightarrow p\bar{p})K^+\pi^-$ contribution from the nonresonant (NR) component, $B^0 \rightarrow p\bar{p}K^+\pi^-$. The ranges of the fits are 5220–5340 MeV and 2908–3058 MeV for the $p\bar{p}K^+\pi^-$ and $p\bar{p}$ mass distributions, respectively.

The ROOFIT package [54] is used to perform the fit separately for the Run 1 and Run 2 data samples. The

Table 1 Yields of the signal and background components from the two-dimensional mass fit to the $m_{p\bar{p}K^+\pi^-}$ and $m_{p\bar{p}}$ distributions for the Run 1 and Run 2 samples in the $p\bar{p}$ mass region of the η_c resonance

Component	Yields	
	Run 1	Run 2
$B^0 \rightarrow \eta_c K^+\pi^-$	772 ± 70	4266 ± 139
$B^0 \rightarrow p\bar{p}K^+\pi^-$	168 ± 69	823 ± 139
Combinatorial background	361 ± 34	1665 ± 68

$m_{p\bar{p}K^+\pi^-}$ distributions of $B^0 \rightarrow \eta_c K^+\pi^-$ signal and $B^0 \rightarrow p\bar{p}K^+\pi^-$ NR decays are both described by a Hypatia probability density functions (PDF) [55] using the same parametrisation. The $m_{p\bar{p}}$ mass distribution of the $B^0 \rightarrow \eta_c K^+\pi^-$ signal decays is described by a relativistic Breit–Wigner (RBW) convolved with a Crystal Ball function [56], while that of the NR contribution is described by an exponential function. The $m_{p\bar{p}K^+\pi^-}$ and $m_{p\bar{p}}$ distributions of the combinatorial background are modelled using exponential functions. A possible component where η_c mesons are combined with random kaons and pions from the PV is investigated but found to be negligible. The meson peak positions, widths, slopes of the exponential functions, and yields, are free to vary in the mass fits while the shape parameters of the signal component are fixed from simulation. The yields of all fit components are

Table 2 Yields of the normalisation and background components from the two-dimensional joint mass fit to the $m_{p\bar{p}K^+\pi^-}$ and $m_{p\bar{p}}$ distributions for the Run 1 and Run 2 samples in the $p\bar{p}$ mass region of the J/ψ resonance

Component	Yields	
	Run 1	Run 2
$B^0 \rightarrow J/\psi K^+\pi^-$	2258 ± 50	12787 ± 119
Combinatorial background	306 ± 24	1496 ± 54

reported in Table 1. Figure 2 shows the projections of the mass fits for the Run 1 and Run 2 samples.

A fit to the $m_{p\bar{p}}$ distribution is also performed incorporating a possible interference term between the NR and the η_c components. This term is found to be consistent with zero and is therefore neglected in the subsequent analysis. In order to test if local interferences are present, the $m_{p\bar{p}}$ distribution is studied in different bins of helicity angles of the $K^+\pi^-$ system. No evidences of local interferences are observed.

3.2 Signal yield of the $B^0 \rightarrow J/\psi K^+\pi^-$ decay

A similar two-dimensional fit procedure is also used to extract the yield of $B^0 \rightarrow J/\psi K^+\pi^-$ decays. A Hypatia PDF is used to parametrise the $J/\psi \rightarrow p\bar{p}$ decay in the range

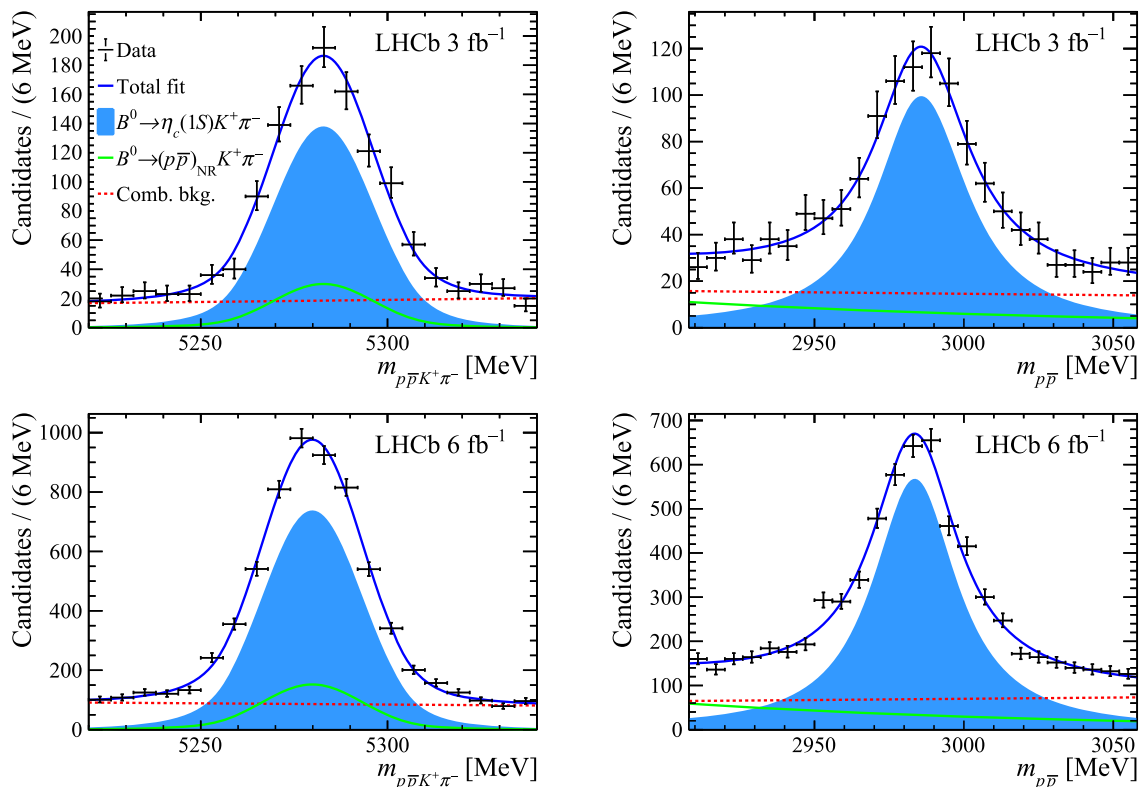


Fig. 2 Results of the two-dimensional mass fit to the (left) $m_{p\bar{p}K^+\pi^-}$ and (right) $m_{p\bar{p}}$ distributions for the (top) Run 1 and (bottom) Run 2 datasets in the region of the η_c resonance

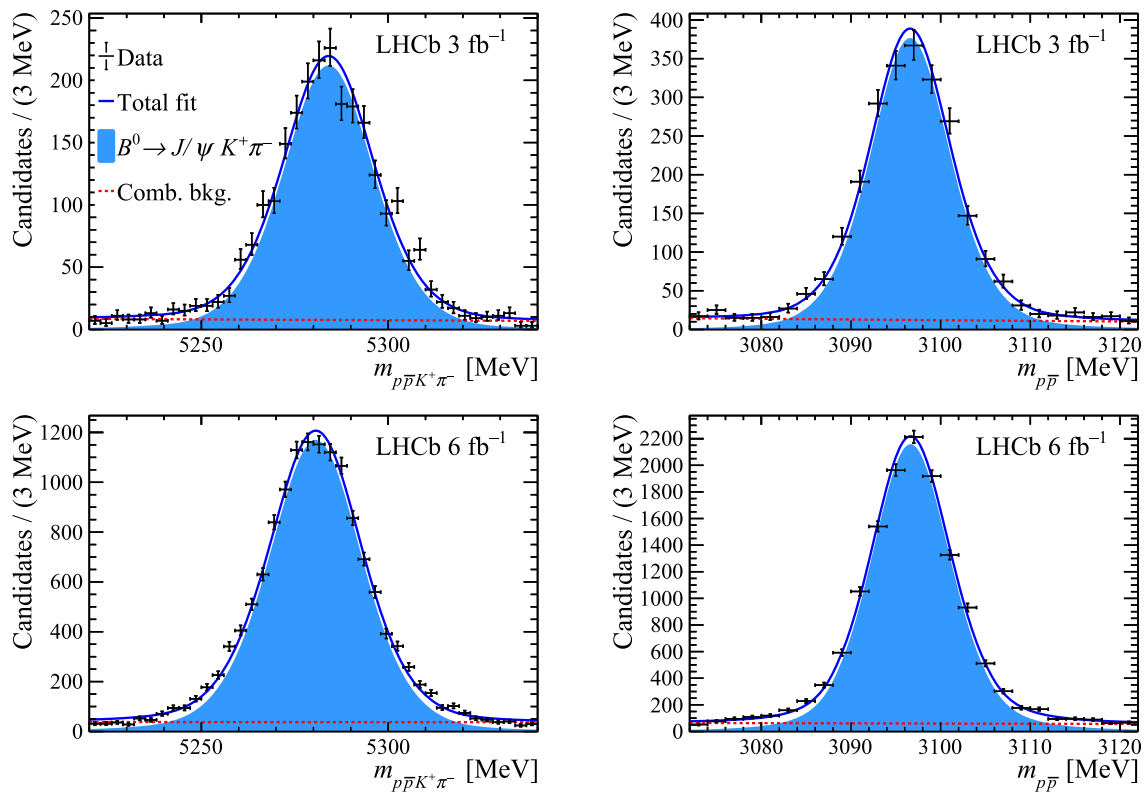


Fig. 3 Results of the two-dimensional fit to the (left) $m_{p\bar{p}K^+\pi^-}$ and (right) $m_{p\bar{p}}$ distributions for the (top) Run 1 and (bottom) Run 2 datasets in the region of the J/ψ resonance

3072–3122 MeV, with the shape parameters fixed from simulation. Nonresonant contributions from $B^0 \rightarrow p\bar{p}K^+\pi^-$ decays are not included in the fit that is used to measure $N_{J/\psi}$, as they are found to be insignificant. The yields of the fit components are reported in Table 2, while the results of the mass fits in the $m_{p\bar{p}}$ mass region of the J/ψ resonance is shown in Fig. 3.

4 Dalitz plot fit

Using the *sPlot* technique [57] applied to the results of the two-dimensional mass fit in the region of the η_c resonance, the background-subtracted DP is determined and shown in Fig. 4.

The phase space for a three-body decay involving only pseudoscalar particles can be represented by a DP, where two of the three possible two-body mass-squared combinations, in this case $m_{K^+\pi^-}^2$ and $m_{\eta_c\pi^-}^2$, define the DP axes. Due to the sizeable natural width of the η_c meson, the p and \bar{p} momenta and energies are used instead of fixing the η_c mass to its known value [49] to compute kinematic quantities such as $m_{\eta_c K^+}^2$, $m_{\eta_c\pi^-}^2$, and the helicity angles.

The formalism used in this analysis follows the approach described in Ref. [20] where an unbinned maximum-

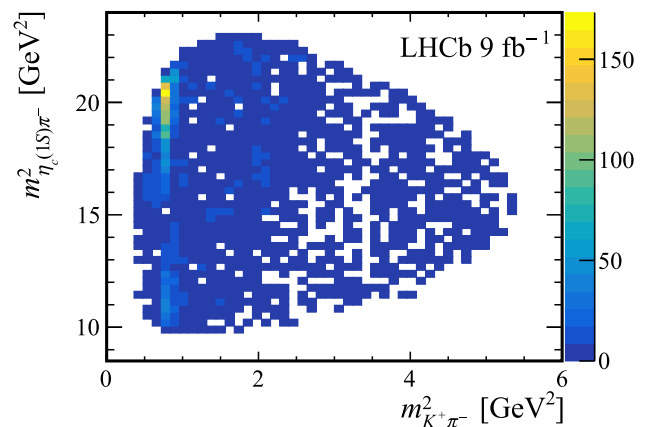


Fig. 4 Background-subtracted DP distribution of the $B^0 \rightarrow \eta_c K^+\pi^-$ decay

likelihood fit on the DP is performed employing the LAURA++ package [58]. The Run 1 and Run 2 subsamples are fitted simultaneously within the JFIT framework [59], with shared free parameters in the DP fit; however, the signal and background yields, as well as the efficiency-variation maps across the phase space, are treated separately for the two datasets.

In the DP fit, the signal corresponds to $B^0 \rightarrow \eta_c K^+\pi^-$ decays, while the background includes both combinatorial

Table 3 Resonances included in the baseline model, where parameter values, uncertainties and spin-parity J^P are taken from Ref. [49]. The lineshapes used are also reported

K^{*0} resonance	Mass [MeV]	Width [MeV]	J^P	Lineshape
$K^*(892)^0$	895.55 ± 0.20	47.3 ± 0.5	1^-	RBW
$K^*(1410)^0$	1414 ± 15	232 ± 21	1^-	RBW
$K_0^*(1430)^0$	1425 ± 50	270 ± 80	0^+	LASS
$K_2^*(1430)^0$	1432.4 ± 1.3	109 ± 5	2^+	RBW
$K^*(1680)^0$	1718 ± 18	320 ± 110	1^-	RBW
$K_0^*(1950)^0$	1957 ± 14	170 ± 50	0^+	RBW

contributions and NR contributions. The likelihood function is given by

$$\mathcal{L} = e^{-\sum_k N_k} \prod_i \left[\sum_k N_k \mathcal{P}_k(m_{K^+\pi^-}^2, m_{\eta_c\pi^-}^2)_i \right], \quad (1)$$

where the index i runs over the number of candidates, while k indexes the signal and background components, with N_k representing their respective yields. The PDFs for the signal and background components are denoted by \mathcal{P}_k , for which the signal PDF is defined as the normalised squared amplitudes scaled by an efficiency model in the DP. Combinatorial and NR background shapes are extracted from the mass fits using the *sPlot* method. These histograms are also interpolated with a cubic spline before the DP fit.

To mitigate issues arising from imperfect efficiency parametrisation at the DP boundaries, a veto is applied to both the lower and upper edges of the DP, effectively excluding regions where any of the masses, $m_{\eta_c\pi^-}$, $m_{\eta_c K^+}$, or $m_{K^+\pi^-}$, are within 70 MeV of their kinematic limits. This veto is also used in both the determination of signal and background yields and the PDF modelling the background.

The mass resolution of the $K^+\pi^-$ system is approximately 5 MeV, which is significantly smaller than the natural width of the narrowest resonance in the Dalitz plot, the $K^*(892)^0$ meson, whose width is about 50 MeV. Therefore, resolution effects are negligible and are not considered further. To ensure convergence to the global minimum, the DP fits are repeated multiple times with randomised initial parameter values.

4.1 Signal efficiency evaluation

In order to perform the DP fit of the $B^0 \rightarrow \eta_c K^+\pi^-$ decay channel, the efficiency variations across the phase space of the decay must be taken into account. Relative variations in efficiency arise from both experimental effects and selection requirements. Efficiencies are calculated on a two-dimensional map parametrised by the variables m' and θ'

Table 4 Parameters of the LASS function resulting from the best fit using the baseline model, where the uncertainties are statistical only

Parameter	Value
r	$4.0 \pm 1.0 \text{ GeV}^{-1}$
a	$4.3 \pm 0.8 \text{ GeV}^{-1}$
$m_{K_0^*(1430)}$	$1434 \pm 22 \text{ MeV}$
$\Gamma_{K_0^*(1430)}$	$409 \pm 44 \text{ MeV}$

which are defined as

$$m' \equiv \frac{1}{\pi} \arccos \left(2 \frac{m_{K^+\pi^-} - m_{K^+\pi^-}^{\min}}{m_{K^+\pi^-}^{\max} - m_{K^+\pi^-}^{\min}} - 1 \right), \quad (2)$$

$$\theta' \equiv \frac{1}{\pi} \theta_{K^+\pi^-}, \quad (3)$$

where the helicity angle $\theta_{K^+\pi^-}$ is defined as the angle between the K^+ and the η_c particles in the $K^+\pi^-$ rest frame. This parametrisation is used to obtain a square Dalitz plot which mitigates potential issues related to the otherwise curved boundaries in the $m_{K^+\pi^-}^2$ and $m_{\eta_c\pi^-}^2$ space and the finite width of the η_c resonance. The phase-space boundaries of the $K^+\pi^-$ mass are represented by $m_{K^+\pi^-}^{\min}$ and $m_{K^+\pi^-}^{\max}$.

The efficiency distributions are computed using simulation as two-dimensional histograms in the square DP space, using the four-momenta of the final-state particles. These momenta are obtained from a fit with the selected B^0 candidates, where the B^0 mass is constrained to its known value [49] and its direction required to point towards the associated primary vertex. The efficiency distributions are calculated by applying the full event selection, where potential discrepancies arising from trigger, tracking, and B^0 -kinematic sources are found to be negligible. The effect of the vetoes in the phase space is separately accounted for by the LAURA++ package, setting the signal efficiency to zero both within the excluded regions and beyond the phase-space border restrictions. The histograms modelling the efficiency undergo a smoothing procedure through cubic-spline interpolation in order to reduce the statistical fluctuations due to the limited size of the simulated samples and are studied separately for the Run 1 and Run 2 samples.

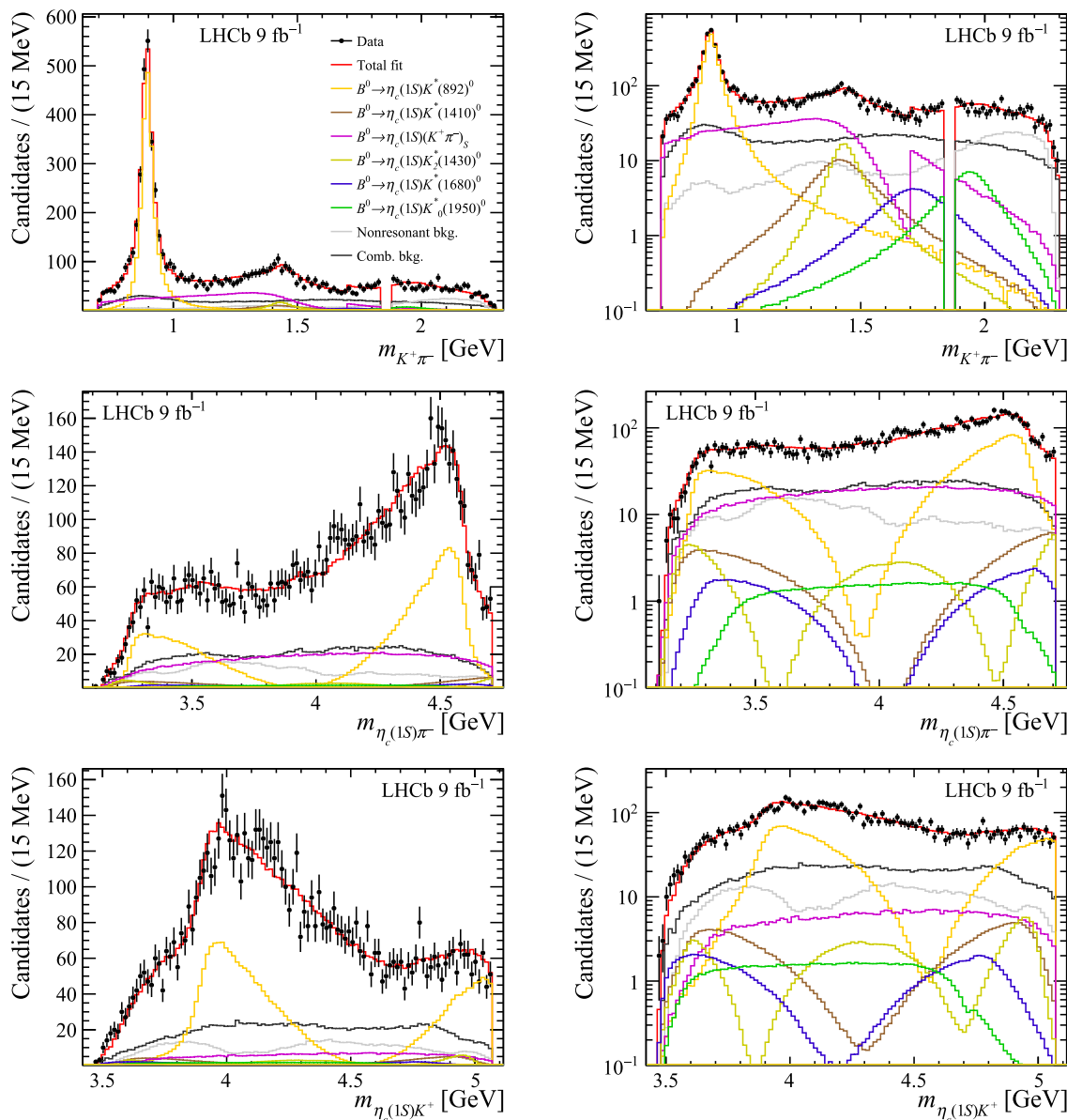


Fig. 5 Projections of the $B^0 \rightarrow \eta_c K^+ \pi^-$ data and DP fit using the baseline model onto the (top) $m_{K^+ \pi^-}$, (middle) $m_{\eta_c \pi^-}$ and (bottom) $m_{\eta_c K^+}$ observables for (left) linear and (right) logarithmic vertical-axis scale. The veto of $B^0 \rightarrow p \bar{p} \bar{D}^0$ decays is visible in the projections onto the $m_{K^+ \pi^-}$ observable

Table 5 Magnitudes, phases and fit fractions determined from the DP fit using the baseline model, where the uncertainties are statistical only

Amplitude	Magnitude	Phase	Fit fraction (%)
$B^0 \rightarrow \eta_c K^*(892)^0$	1 (fixed)	0 (fixed)	49.3 ± 1.2
$B^0 \rightarrow \eta_c K^*(1410)^0$	0.30 ± 0.04	-0.14 ± 0.13	4.5 ± 1.4
$B^0 \rightarrow \eta_c K_0^*(1430)^0$	0.79 ± 0.04	$+2.94 \pm 0.05$	30.8 ± 4.7
$B^0 \rightarrow \eta_c (K^+ \pi^-)_{\text{SVP}}$	0.56 ± 0.03	$+2.81 \pm 0.07$	15.4 ± 2.4
$B^0 \rightarrow \eta_c K_2^*(1430)^0$	0.28 ± 0.03	-0.73 ± 0.10	3.7 ± 0.9
$B^0 \rightarrow \eta_c K^*(1680)^0$	0.21 ± 0.05	$+0.21 \pm 0.22$	2.1 ± 0.9
$B^0 \rightarrow \eta_c K_0^*(1950)^0$	0.22 ± 0.03	$+1.53 \pm 0.29$	2.4 ± 0.5
Sum of fit fractions			108.2 ± 3.1

4.2 Amplitude model with only K^{*0} resonances

The established $K^{*0} \rightarrow K^+\pi^-$ mesons, reported in Ref. [49], satisfying $m_{K^*} \lesssim m_{B^0} - m_{\eta_c}$, i.e. with masses within or slightly above the phase-space boundary in $B^0 \rightarrow \eta_c K^+\pi^-$ decays, serve as a guide when building the model. Only contributions that significantly improve the data description are included. This model, referred to as the baseline model, comprises the resonances shown in Table 3, with their masses and widths fixed to their known values [49], except for the $K_0^*(1430)^0$ as described later. In the DP fit, the signal and background yields are fixed to the values obtained from the two-dimensional mass fit. The effect of the phase-space boundary cut on these yields is negligible.

The $K^*(892)^0$ resonance serves as a reference amplitude, with its magnitude fixed to unity and phase set to zero. The complex coefficients [60–62] of the remaining contributions are determined relative to those of the $K^*(892)^0$ meson. The low-mass $(K^+\pi^-)_S$ S-wave is modelled with the LASS function [63]. The scattering length (a) and the effective range (r) parametrising the slowly varying part (SVP) of the LASS function are left free to vary in the fit. The resonance mass and width are constrained with Gaussian priors centred on their known values [49]. Once the global minimum of the negative log-likelihood is reached, the four parameters reported in Table 4 are fixed to their best-fit values and then the fits are repeated. This procedure negates the recalculation of resonant lineshapes in the function minimisation loop, ensuring faster convergence. The remaining resonances in the fit are modelled using RBW lineshapes, with their Blatt–Weisskopf barrier-factor radii fixed at 4 GeV^{-1} . The addition of the $K_3^*(1780)$ and $K_4^*(2045)$ mesons are found to be not significant and therefore not included in the model.

A good description of the $m_{K^+\pi^-}$ and $m_{\eta_c K^+}$ mass distributions with only K^{*0} contributions is generally achieved. However, discrepancies between data and fit projections onto the $m_{\eta_c \pi^-}$ and $m_{\eta_c K^+}$ distributions are visible around $m_{\eta_c \pi^-} \sim 4.1 \text{ GeV}$ and $m_{\eta_c K^+} \sim 4.1 \text{ GeV}$, as shown in Fig. 5. The values of the magnitudes, phases and fit fractions for each contribution are reported in Table 5. A χ^2 variable is computed on the squared DP to quantitatively assess the fit quality, using an adaptive two-dimensional binning scheme that ensures at least 20 events per bin, corresponding to 324 bins. For the baseline model and binning scheme, the goodness of the fit is $\chi^2/\text{ndf} = 425/309$, where ndf is the number of degrees of freedom.

Two additional validation checks are performed. First, a mixed-sample unbinned goodness-of-fit test [64] is used to remove binning effects; the fit to the resulting test statistic yields $\chi^2/\text{ndf} = 22.6/21$, consistent with good agreement between data and model. Second, 1000 pseudoexperiments are generated and fitted with the nominal procedure. For each pseudoexperiment a χ^2/ndf value is computed as described

above, and the p-value is defined as the fraction of pseudoexperiments with χ^2/ndf larger than that observed in data. Neglecting systematic uncertainties, this procedure gives a p-value of 3.1%.

4.3 Amplitude model with K^{*0} resonances and an $\eta_c \pi^-$ exotic contribution

A better description of the data, compared to the previous model, is sought by adding to the baseline model an amplitude corresponding to an exotic candidate, $T_{c\bar{c}}(4100)^- \rightarrow \eta_c \pi^-$ which is described by a RBW, in addition to the K^{*0} resonances listed in Table 3. In addition to the parameters that are free in the baseline model, the complex coefficients, and RBW mass and width of the exotic candidate are left free to vary. The strategy followed for the LASS parameters is the same as described before ensuring faster convergence times when an exotic contribution is included in the model. The values found from the best fit for the LASS function and the exotic candidate are reported in Table 6. A likelihood-ratio test, based on the log-likelihood difference with respect to the baseline value, $\Delta(-2 \ln \mathcal{L})$ [65], is used to compare different amplitude models. The exotic candidate is tested under two quantum-number hypotheses, repeating the DP fit for the $J^P = 0^+$ and 1^- assignments. The corresponding $\Delta(-2 \ln \mathcal{L})$ values, are 16.2 and 29.0, respectively. Thus, the model providing the best description of data, referred to as the extended fit model, is obtained with the addition of an exotic candidate with $J^P = 1^-$.

The values for the magnitude, phase and fit fraction of each contribution are reported in Table 7. Statistical uncertainties on the fit fractions are determined using large samples of pseudoexperiments generated from the fit results, thereby accounting for correlations between parameters. The mass projections of the extended model are shown in Fig. 6, for which the value of the χ^2/ndf is 401/305. The fit quality is further assessed comparing the unnormalised Legendre moments between background-subtracted data and the model.

The significance of the $T_{c\bar{c}}(4100)^-$ candidate is evaluated from the value of $\Delta(-2 \ln \mathcal{L})$, assuming that this quantity follows a χ^2 distribution with degrees of freedom equal to twice the number of free parameters in its expression [66–68]. This assumption accounts for the look-elsewhere effect due to the varying mass and width of the $T_{c\bar{c}}(4100)^-$ candidate. Its validity is verified through pseudoexperiments, which test the $\Delta(-2 \ln \mathcal{L})$ distribution under the baseline hypothesis. The results confirm that this distribution is well described by a χ^2 function with 8 degrees of freedom. In the extended fit model, the statistical significance of the $T_{c\bar{c}}(4100)^-$ is found to be 3.6 standard deviations (σ), excluding systematic uncertainties. To distinguish between different J^P assignments, fits are performed under alternative J^P hypotheses. A lower

Table 6 Parameters of the LASS function and the exotic $J^P = 1^-$ candidate resulting from the best fit using the extended model

Parameter	Value	Lineshape
r	$4.6 \pm 1.0 \text{ GeV}^{-1}$	LASS
a	$4.2 \pm 0.7 \text{ GeV}^{-1}$	LASS
$m_{K_0^*(1430)}$	$1433 \pm 19 \text{ MeV}$	LASS
$\Gamma_{K_0^*(1430)}$	$359 \pm 37 \text{ MeV}$	LASS
$m_{T_{c\bar{c}}(4100)^-}$	$4106 \pm 23 \text{ MeV}$	RBW
$\Gamma_{T_{c\bar{c}}(4100)^-}$	$506 \pm 166 \text{ MeV}$	RBW

limit on the significance of rejecting the $J^P = 0^+$ hypothesis is determined from the change in the log-likelihood relative to the preferred hypothesis, assuming a χ^2 distribution with one degree of freedom. This assumption is similarly validated using pseudoexperiments, which confirm that the $\Delta(-2 \ln \mathcal{L})$ distribution under the disfavoured $J^P = 0^+$ hypothesis follows the expected χ^2 behaviour. The $J^P = 0^+$ hypothesis with respect to that of $J^P = 1^-$ is statistically disfavoured at 3.2σ . However, systematic effects must be taken into account to determine the significance of the $T_{c\bar{c}}(4100)^-$ contribution and the discrimination of its quantum numbers.

4.4 Systematic uncertainties

Systematic uncertainties on the fit fractions, amplitude, and phases are evaluated by measuring the difference between the baseline value and the value obtained from different studies as detailed below.

The systematic uncertainties associated with the background model are evaluated using alternative histograms, obtained by randomly varying the bin contents within their statistical uncertainties before spline interpolation. Approximately 1000 such histograms are generated for both the combinatorial and NR background components and used to construct an equal number of pseudoexperiments, where the signal contribution is generated according to the baseline model. Each pseudoexperiment is fitted with the baseline signal model and the corresponding modified background model, and the systematic uncertainty on the fit fractions is taken as the standard deviation of the resulting distribution of best-fit values, which is well described by a Gaussian. The same pseudoexperiments are also used to estimate the significance of the $T_{c\bar{c}}(4100)^-$ state. Each is fitted twice: once with the baseline model and once with the extended model, both including the varied background maps. The resulting distribution of $\Delta(-2 \ln \mathcal{L})$ values does not follow a χ^2 distribution. A p -value is therefore determined from the fraction of fits yielding a $\Delta(-2 \ln \mathcal{L})$ greater than that

observed in data, corresponding to 1.45%, or a significance of 2.5σ .

The strategy used to assess the systematic uncertainty associated to the background model is also adopted to account for the effects relating to the efficiency model. Another systematic uncertainty is associated to the veto applied to the DP borders. The DP fit is repeated removing these vetoes.

The statistical uncertainties of signal and background yields are incorporated by applying constraints with Gaussian priors and repeating the fit to account for variations within these uncertainties.

A systematic uncertainty related to the potential fit bias is determined using pseudoexperiments. Samples are generated according to the baseline fit result and fitted again. The associated error is calculated as the squared sum of the residuals and the standard deviation.

The kinematic variables used in the DP fit are computed from the B^0 -meson and final-state-particle four-momenta. In order to associate a systematic uncertainty to the η_c natural width, the DP fits are repeated with kinematic variables that are recomputed assigning to the η_c mass the values $m_{\eta_c} \pm \Gamma_{\eta_c}/2$, where m_{η_c} and Γ_{η_c} are the mass and natural width of the η_c meson, respectively, obtained from the mass fits reported in Sect. 3.1.

In the baseline model the K^{*0} resonances are modelled by RBW functions with their mass and width parameters fixed to known values [49], and with fixed Blatt–Weisskopf barrier factor radii. The uncertainties related to this choice are determined by varying simultaneously and randomly the masses and widths within their uncertainties and, separately, by changing the radii between 3 and 5 GeV^{-1} .

The LASS model used to parametrise the low-mass $K^+\pi^-$ S-wave in the baseline fit is replaced with $K_0^*(1430)^0$ and $K_0^*(700)^0$ resonances parametrised by RBW functions, and a NR S-wave $K^+\pi^-$ component parametrised with a uniform amplitude.

When including these sources of systematic uncertainties, summarised in Table 8, the $T_{c\bar{c}}(4100)^-$ contribution is not found to be significant. Only the significances that deviate most from the nominal value are shown and the background parametrisation is found to be dominant. For this reason, systematic uncertainties associated to the mass and width of the $T_{c\bar{c}}(4100)^-$ candidate, and on the discrimination between quantum-number hypotheses, are not assigned.

The baseline model is therefore used to compute the branching fractions of the K^{*0} contributions in order to characterise the $B^0 \rightarrow \eta_c K^+\pi^-$ decay channel. To this end, the extended model is also considered as an alternative to the baseline model, with associated systematic uncertainties. The addition of a resonance decaying to $\eta_c K^+$ was initially considered, but it was consistently found to be less significant than the one decaying to $\eta_c \pi^-$. Therefore, it was not pursued

Table 7 Magnitudes, phases and fit fractions determined from the DP fit using the extended model. Uncertainties are statistical only

Amplitude	Magnitude	Phase	Fit fraction (%)
$B^0 \rightarrow \eta_c K^*(892)^0$	1 (fixed)	0 (fixed)	49.1 ± 1.3
$B^0 \rightarrow \eta_c K^*(1410)^0$	0.28 ± 0.03	-0.04 ± 0.15	3.9 ± 0.9
$B^0 \rightarrow \eta_c K_0^*(1430)^0$	0.73 ± 0.04	-0.18 ± 0.05	26.2 ± 4.1
$B^0 \rightarrow \eta_c (K^+\pi^-)_{\text{SVP}}$	0.51 ± 0.03	$+0.31 \pm 0.07$	12.9 ± 2.0
$B^0 \rightarrow \eta_c K_2^*(1430)^0$	0.28 ± 0.03	-0.86 ± 0.11	4.0 ± 0.9
$B^0 \rightarrow \eta_c K^*(1680)^0$	0.18 ± 0.05	$+0.32 \pm 0.23$	1.5 ± 0.9
$B^0 \rightarrow \eta_c K_0^*(1950)^0$	0.21 ± 0.03	-0.92 ± 0.35	2.2 ± 0.7
$B^0 \rightarrow T_{c\bar{c}}(4100)^- K^+$	0.15 ± 0.03	-3.14 ± 0.06	1.1 ± 0.5
Sum of fit fractions			100.9 ± 3.5

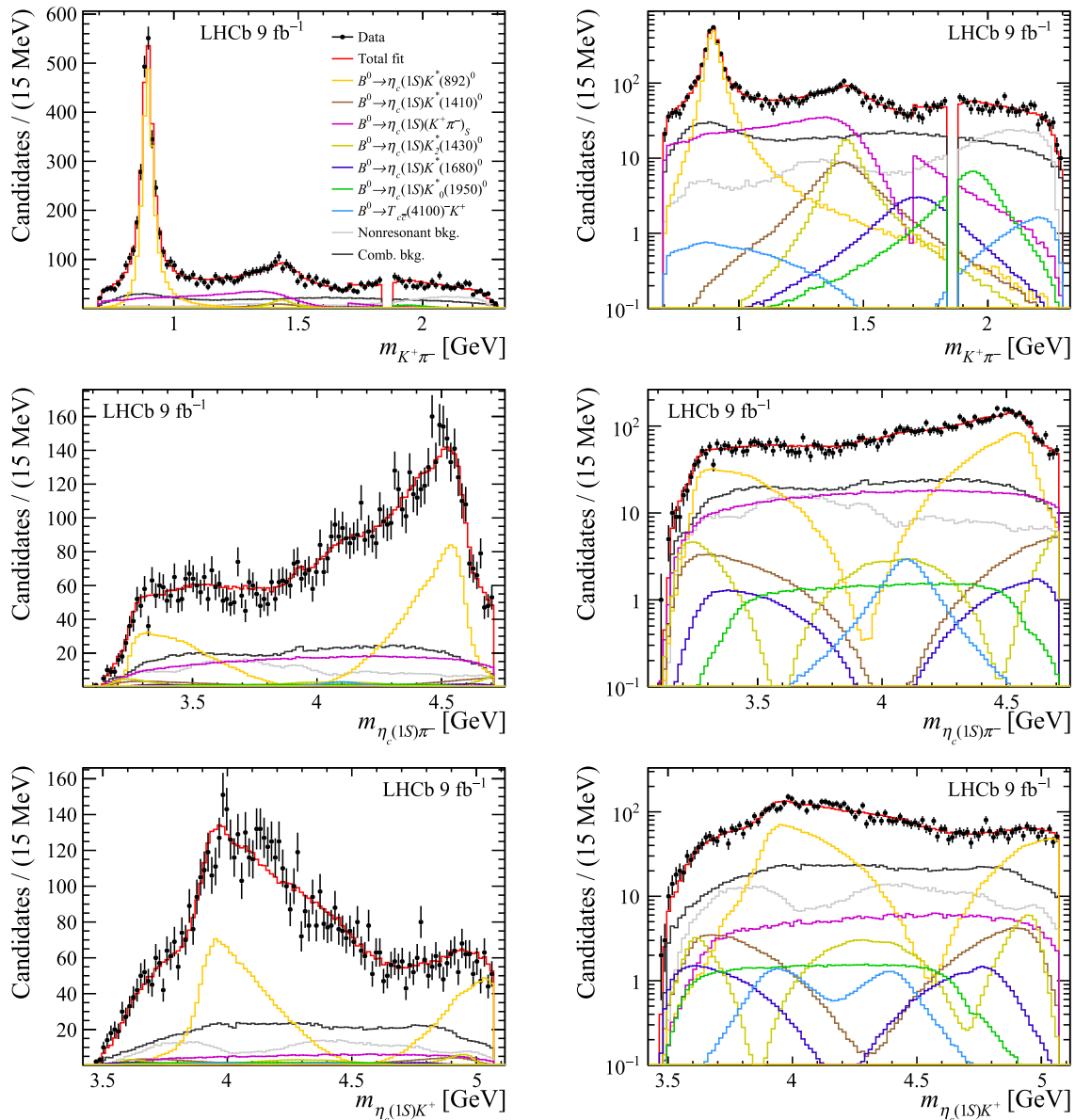


Fig. 6 Projections of the $B^0 \rightarrow \eta_c K^+ \pi^-$ data and DP fit using the extended model onto the (top) $m_{K^+ \pi^-}$, (middle) $m_{\eta_c \pi^-}$ and (bottom) $m_{\eta_c K^+}$ observables for (left) linear and (right) logarithmic vertical-axis scale. The veto of $B^0 \rightarrow p \bar{p} D^0$ decays is visible in the projections onto the $m_{K^+ \pi^-}$ observable

Table 8 Significance of the extended model (with the $T_{c\bar{c}}(4100)^-$ candidate) with respect to the baseline model (without the $T_{c\bar{c}}(4100)^-$ candidate) for the main sources of systematic uncertainty

Source	Significance
Background parametrisation	2.5σ
Efficiency parametrisation	4.1σ
DP-border veto	3.2σ
Fixed yields	3.2σ
η_c natural width	3.0σ
Fixed K^{*0} lineshape parameters	3.2σ
$K^+\pi^-$ S-wave	4.5σ

further. The values for the fit fractions of the K^{*0} components and their interference fit fractions, together with their associated systematic uncertainties, are reported in Table 9, while the magnitudes and phases are given in Table 10.

5 Branching fraction measurement

The measurement of the inclusive $B^0 \rightarrow \eta_c K^+\pi^-$ branching fraction is performed relative to the normalisation channel $B^0 \rightarrow J/\psi K^+\pi^-$. The absolute branching fraction of the $B^0 \rightarrow \eta_c K^+\pi^-$ decay can then be calculated using the relation

$$\mathcal{B}(B^0 \rightarrow \eta_c K^+\pi^-) = \mathcal{B}(B^0 \rightarrow J/\psi K^+\pi^-) \times \frac{\mathcal{B}(J/\psi \rightarrow p\bar{p})}{\mathcal{B}(\eta_c \rightarrow p\bar{p})} \frac{N_{\eta_c}}{N_{J/\psi}} \frac{\epsilon_{J/\psi}}{\epsilon_{\eta_c}}, \tag{4}$$

where $\mathcal{B}(B^0 \rightarrow J/\psi K^+\pi^-) = (1.15 \pm 0.05) \times 10^{-3}$, $\mathcal{B}(J/\psi \rightarrow p\bar{p}) = (2.120 \pm 0.029) \times 10^{-3}$ and $\mathcal{B}(\eta_c \rightarrow p\bar{p}) = (1.33 \pm 0.11) \times 10^{-3}$ are taken as external inputs [49]. The values N_{η_c} and $N_{J/\psi}$ are the respective yields of the $B^0 \rightarrow \eta_c K^+\pi^-$ and $B^0 \rightarrow J/\psi K^+\pi^-$ contributions, as reported in Tables 1 and 2, while $\epsilon_{J/\psi}$ and ϵ_{η_c} are the selection efficiencies of the signal and normalisation channel calculated from simulation.

Selection efficiencies are determined from the $B^0 \rightarrow \eta_c K^+\pi^-$ and $B^0 \rightarrow J/\psi K^+\pi^-$ simulated samples, both selected using the same criteria as applied to data. Weights are applied to the simulated candidates to correct for minor discrepancies with respect to data, based on track multiplicity, B^0 kinematic distributions, and the respective DP distributions. Discrepancies due to the trigger responses are investigated and found to be negligible. The ratio of efficiencies is given by $\epsilon_{J/\psi}/\epsilon_{\eta_c} = 0.945 \pm 0.004$ for Run 1 and $\epsilon_{J/\psi}/\epsilon_{\eta_c} = 0.948 \pm 0.003$ for Run 2, where the uncertainties are statistical.

Systematic uncertainties on the branching fraction measurement are evaluated by recomputing the signal and normalisation yields, along with their efficiency ratios, for each

Table 9 Symmetric matrix of the fit fractions and interference fit fractions (%) resulting from the fit using the baseline model, where the quoted uncertainties are statistical and systematic, respectively. Entries

	$\eta_c K^*(892)^0$	$\eta_c K^*(1410)^0$	$\eta_c K_0^*(1430)^0$	$\eta_c(K^+\pi^-)_{\text{SVP}}$	$\eta_c K_2^*(1430)^0$	$\eta_c K^*(1680)^0$	$\eta_c K_0^*(1950)^0$
$\eta_c K^*(892)^0$	$49.3 \pm 1.2^{+3.8}_{-3.4}$	$-2.1 \pm 1.8^{+3.1}_{-3.3}$	–	–	–	$0.8 \pm 1.2^{+3.7}_{-4.5}$	–
$\eta_c K^*(1410)^0$		$4.5 \pm 1.4^{+3.2}_{-3.1}$	–	–	–	$-3.2 \pm 1.5^{+6.5}_{-2.3}$	–
$\eta_c K_0^*(1430)^0$			$30.8 \pm 4.7^{+5.5}_{-4.3}$	$-10.8 \pm 1.3^{+1.9}_{-1.5}$	–	–	$7.0 \pm 10.3^{+7.9}_{-8.6}$
$\eta_c(K^+\pi^-)_{\text{SVP}}$				$15.4 \pm 2.4^{+2.7}_{-2.2}$	–	–	–
$\eta_c K_2^*(1430)^0$					$3.7 \pm 0.9^{+1.3}_{-2.0}$	–	–
$\eta_c K^*(1680)^0$						$2.1 \pm 0.9^{+1.3}_{-1.7}$	–
$\eta_c K_0^*(1950)^0$							$2.4 \pm 0.5^{+2.7}_{-2.4}$

marked with a dash correspond to instances where the modulus of the interference fit fraction is found to be less than $10^{-4}\%$

Table 10 Magnitudes and phases determined from the DP fit using the baseline model, where the uncertainties are statistical and systematic, respectively

Amplitude	Magnitude	Phase
$B^0 \rightarrow \eta_c K^*(892)^0$	1 (fixed)	0 (fixed)
$B^0 \rightarrow \eta_c K^*(1410)^0$	$0.30 \pm 0.04^{+0.06}_{-0.14}$	$-0.14 \pm 0.13^{+0.57}_{-0.53}$
$B^0 \rightarrow \eta_c K_0^*(1430)^0$	$0.79 \pm 0.04^{+0.17}_{-0.06}$	$+2.94 \pm 0.05^{+0.09}_{-0.10}$
$B^0 \rightarrow \eta_c(K^+\pi^-)_{\text{SVP}}$	$0.56 \pm 0.03^{+0.15}_{-0.07}$	$+2.81 \pm 0.07^{+0.07}_{-0.09}$
$B^0 \rightarrow \eta_c K_2^*(1430)^0$	$0.28 \pm 0.03^{+0.03}_{-0.07}$	$-0.73 \pm 0.10^{+0.19}_{-0.23}$
$B^0 \rightarrow \eta_c K^*(1680)^0$	$0.21 \pm 0.05^{+0.05}_{-0.09}$	$+0.21 \pm 0.22^{+0.59}_{-0.31}$
$B^0 \rightarrow \eta_c K_0^*(1950)^0$	$0.22 \pm 0.03^{+0.09}_{-0.08}$	$+1.53 \pm 0.29^{+0.73}_{-0.55}$

Table 11 Systematic uncertainties on the $B^0 \rightarrow \eta_c K^+ \pi^-$ branching fraction. Statistical uncertainties are also reported for comparison

Source	$\sigma_{\mathcal{B}(B^0 \rightarrow \eta_c K^+ \pi^-)} [10^{-4}]$	
	Run 1	Run 2
Shape parameters	0.05	0.05
Resolution and NR $p\bar{p}$ model	0.18	0.22
Mass windows	0.41	0.15
Total systematic uncertainty	0.45	0.27
Statistical uncertainty	0.53	0.22

source of uncertainty. The difference of the resulting branching fraction from the baseline value is taken as the associated systematic uncertainty. The overall systematic uncertainty is calculated by combining all contributions in quadrature. The contribution arising from fixing the parameters of the Hypatia PDFs used to parametrise the B^0 and J/ψ components, as well as the Crystal Ball PDF for the η_c , is evaluated by repeating the fit with parameter values varied according to a multivariate normal distribution. To assess a systematic uncertainty for the model used to describe the mass resolution, the fits are repeated by replacing the Hypatia PDFs with Crystal Ball PDFs. The convolution of the RBW with a Crystal Ball PDF is replaced by a Voigtian PDF, where the parameters are fixed based on simulation. The $m_{p\bar{p}}$ distribution of the NR component, originally parametrised with an exponential function, is instead modelled with a linear function. The systematic uncertainty related to the choice of the mass ranges in the two-dimensional fit is evaluated by performing fits with alternative ranges. Table 11 summarises the systematic uncertainties.

The measured values of the branching fraction $\mathcal{B}(B^0 \rightarrow \eta_c K^+ \pi^-)$ are $(6.10 \pm 0.53 \pm 0.45 \pm 0.58) \times 10^{-4}$ for Run 1 and $(5.77 \pm 0.22 \pm 0.27 \pm 0.55) \times 10^{-4}$ for Run 2. This leads to the combined value

$$\mathcal{B}(B^0 \rightarrow \eta_c K^+ \pi^-) = (5.82 \pm 0.20 \pm 0.23 \pm 0.55) \times 10^{-4},$$

where the first uncertainty is statistical, the second systematic, and the third is due to the limited knowledge of the external branching fractions. The combined value is obtained as the weighted average of the Run 1 and Run 2 results. This result is in agreement with the world average [49] and with the previous LHCb result [20]. The product branching fractions for the intermediate states contributing to the $B^0 \rightarrow \eta_c K^{*0} (\rightarrow K^+ \pi^-)$ decays listed in Table 12, are determined by scaling the inclusive branching fraction $\mathcal{B}(B^0 \rightarrow \eta_c K^+ \pi^-)$ by the fit fractions of each intermediate state with the baseline model reported in Table 9.

Table 12 Product branching fractions for intermediate K^{*0} resonances decaying to $K^+ \pi^-$ contributing to the $B^0 \rightarrow \eta_c K^{*0} (\rightarrow K^+ \pi^-)$ decay, $\mathcal{B}(B^0 \rightarrow \eta_c K^{*0}) \times \mathcal{B}(K^{*0} \rightarrow K^+ \pi^-)$. The quoted uncertainties are statistical, from the inclusive branching fraction of $B^0 \rightarrow \eta_c K^+ \pi^-$, from the intermediate fit fraction and from the charmonium branching fractions of $\eta_c \rightarrow p\bar{p}$ and $J/\psi \rightarrow p\bar{p}$, respectively

Decay	Branching fraction [10^{-5}]
$B^0 \rightarrow \eta_c K^*(892)^0 (\rightarrow K^+ \pi^-)$	$28.69 \pm 1.21 \pm 1.13^{+2.21}_{-1.98} \pm 2.71$
$B^0 \rightarrow \eta_c K^*(1410)^0 (\rightarrow K^+ \pi^-)$	$2.62 \pm 0.82 \pm 0.10^{+1.86}_{-1.80} \pm 0.25$
$B^0 \rightarrow \eta_c K_0^*(1430)^0 (\rightarrow K^+ \pi^-)$	$17.92 \pm 2.80 \pm 0.71^{+3.26}_{-2.56} \pm 1.69$
$B^0 \rightarrow \eta_c (K^+ \pi^-)_{\text{SVP}}$	$8.96 \pm 1.42 \pm 0.35^{+1.63}_{-1.28} \pm 0.84$
$B^0 \rightarrow \eta_c K_2^*(1430)^0 (\rightarrow K^+ \pi^-)$	$2.15 \pm 0.53 \pm 0.08^{+0.76}_{-1.16} \pm 0.20$
$B^0 \rightarrow \eta_c K^*(1680)^0 (\rightarrow K^+ \pi^-)$	$1.22 \pm 0.52 \pm 0.05^{+0.76}_{-0.99} \pm 0.12$
$B^0 \rightarrow \eta_c K_0^*(1950)^0 (\rightarrow K^+ \pi^-)$	$1.40 \pm 0.29 \pm 0.06^{+1.57}_{-1.40} \pm 0.13$

6 Conclusion

An amplitude analysis of the $B^0 \rightarrow \eta_c(1S)K^+ \pi^-$ decay channel is performed using the dataset collected by LHCb in Run 1 and 2, corresponding to an integrated luminosity of 9 fb^{-1} . While a better description of the data is achieved when including a charged exotic charmonium-like $T_{c\bar{c}}(4100)^-$ candidate decaying to $\eta_c(1S)\pi^-$, the contribution is not significant when systematic uncertainties are taken into account. The results of this analysis are valid in the absence of additional suppressed intermediate resonances decaying to the $B^0 \rightarrow p\bar{p}K^+ \pi^-$ final state, possibly interfering with the amplitudes involved in the $B^0 \rightarrow (\eta_c(1S) \rightarrow p\bar{p})K^+ \pi^-$ decay. Several checks, including the comparison between the Legendre moments computed from data and from the fit models, confirms that, with the current dataset, there is no sensitivity to such interference effects, if present.

A measurement of the inclusive $B^0 \rightarrow \eta_c(1S)K^+ \pi^-$ branching fraction is also performed, as well as the branching fraction measurements of the intermediate K^{*0} resonances contributing to the decay. The results of this analysis, using a data sample size that is approximately doubled with respect to the previous study, supersede those obtained in Ref. [20].

Acknowledgements We express our gratitude to our colleagues in the CERN accelerator departments for the excellent performance of the LHC. We thank the technical and administrative staff at the LHCb institutes. We acknowledge support from CERN and from the national agencies: ARC (Australia); CAPES, CNPq, FAPERJ and FINEP (Brazil); MOST and NSFC (China); CNRS/IN2P3 (France); BMBF, DFG and MPG (Germany); INFN (Italy); NWO (Netherlands); MNiSW and NCN (Poland); MCID/IFA (Romania); MICIU and AEI (Spain); SNSF and SER (Switzerland); NASU (Ukraine); STFC (United Kingdom); DOE NP and NSF (USA). We acknowledge the computing resources that are provided by ARDC (Australia), CBPF (Brazil), CERN, IHEP and LZU (China), IN2P3 (France), KIT and DESY (Germany), INFN (Italy), SURF (Netherlands), Polish WLCG (Poland), IFIN-HH (Roma-

nia), PIC (Spain), CSCS (Switzerland), and GridPP (United Kingdom). We are indebted to the communities behind the multiple open-source software packages on which we depend. Individual groups or members have received support from Key Research Program of Frontier Sciences of CAS, CAS PIFI, CAS CCEPP, Fundamental Research Funds for the Central Universities, and Sci. & Tech. Program of Guangzhou (China); Minciencias (Colombia); EPLANET, Marie Skłodowska-Curie Actions, ERC and NextGenerationEU (European Union); A*MIDEX, ANR, IPhU and Labex P2IO, and Région Auvergne-Rhône-Alpes (France); Alexander-von-Humboldt Foundation (Germany); ICSC (Italy); Severo Ochoa and María de Maeztu Units of Excellence, GVA, XuntaGal, GENCAT, InTalent-Inditex and Prog. Atracción Talento CM (Spain); SRC (Sweden); the Leverhulme Trust, the Royal Society and UKRI (United Kingdom).

Data Availability Statement Data cannot be made available for reasons disclosed in the data availability statement. [Authors' comment: The LHCb experiment has agreed to the CERN open data policy that is summarised in <https://opendata.cern.ch/docs/about>. In particular, Level 1 data associated with this publication are made available on the CERN document server at <https://cds.cern.ch/record/2941763>. These data contain material related to the paper that allows a reinterpretation of the results in the context of new theoretical models. Level 3 data are also available from the CERN open data portal, but due to the large amount of data, only the Run1 dataset has been made public up to now.]

Code Availability Statement Code/software cannot be made available for reasons disclosed in the code availability statement. [Authors' comment: Software/Code that is associated with this publication and that is publicly available is referenced within the publication content. Specific analysis software/code used to produce the results shown in the publication is preserved within the LHCb collaboration internally and can be provided on reasonable request, provided it doesn't contain information that can be associated with unpublished results.]

Open Access This article is licensed under a Creative Commons Attribution 4.0 International License, which permits use, sharing, adaptation, distribution and reproduction in any medium or format, as long as you give appropriate credit to the original author(s) and the source, provide a link to the Creative Commons licence, and indicate if changes were made. The images or other third party material in this article are included in the article's Creative Commons licence, unless indicated otherwise in a credit line to the material. If material is not included in the article's Creative Commons licence and your intended use is not permitted by statutory regulation or exceeds the permitted use, you will need to obtain permission directly from the copyright holder. To view a copy of this licence, visit <http://creativecommons.org/licenses/by/4.0/>.

Funded by SCOAP³.

References

1. M. Gell-Mann, A schematic model of baryons and mesons. Phys. Lett. **8**, 214 (1964). [https://doi.org/10.1016/S0031-9163\(64\)92001-3](https://doi.org/10.1016/S0031-9163(64)92001-3)
2. G. Zweig, An SU₃ model for strong interaction symmetry and its breaking; Version 1. <http://cds.cern.ch/record/352337>. CERN-TH-401, CERN, Geneva (1964)
3. Belle Collaboration, S.-K. Choi et al., Observation of a narrow charmonium-like state in exclusive $B^\pm \rightarrow K^\pm \pi^+ \pi^- J/\psi$ decays. Phys. Rev. Lett. **91**, 262001 (2003). <https://doi.org/10.1103/PhysRevLett.91.262001>. arXiv:hep-ex/0309032
4. Belle Collaboration, A. Bondar et al., Observation of two charged bottomonium-like resonances in $Y(5S)$ decays. Phys. Rev. Lett.

- 108, 122001 (2012). <https://doi.org/10.1103/PhysRevLett.108.122001>. arXiv:1110.2251
5. Belle Collaboration, K. Abe et al., Observation of a near-threshold $\omega J/\psi$ mass enhancement in exclusive $B \rightarrow K \omega J/\psi$ decays. Phys. Rev. Lett. **94**, 182002 (2005). <https://doi.org/10.1103/PhysRevLett.94.182002>. arXiv:hep-ex/0408126
6. CLEO Collaboration, T.E. Coan et al., Charmonium decays of $Y(4260)$, $\psi(4160)$ and $\psi(4040)$. Phys. Rev. Lett. **96**, 162003 (2006). <https://doi.org/10.1103/PhysRevLett.96.162003>. arXiv:hep-ex/0602034
7. CDF Collaboration, T. Aaltonen et al., Observation of the $Y(4140)$ Structure in the $J/\psi \phi$ Mass Spectrum in $B^\pm \rightarrow J/\psi \phi K^\pm$ Decays. Mod. Phys. Lett. A **32**, 1750139 (2017). <https://doi.org/10.1142/S0217732317501395>. arXiv:1101.6058
8. M. Karliner, J.L. Rosner, New exotic meson and baryon resonances from doubly heavy hadronic molecules. Phys. Rev. Lett. **115**, 122001 (2015). <https://doi.org/10.1103/PhysRevLett.115.122001>. arXiv:1506.06386
9. L. Maiani, F. Piccinini, A.D. Polosa, V. Riquer, Diquark-antidiquarks with hidden or open charm and the nature of $X(3872)$. Phys. Rev. D **71**, 014028 (2005). <https://doi.org/10.1103/PhysRevD.71.014028>. arXiv:hep-ph/0412098
10. L. Maiani, A.D. Polosa, V. Riquer, The new pentaquarks in the diquark model. Phys. Lett. B **749**, 289 (2015). <https://doi.org/10.1016/j.physletb.2015.08.008>. arXiv:1507.04980
11. S. Dubynskiy, M.B. Voloshin, Hadro-charmonium. Phys. Lett. B **666**, 344 (2008). <https://doi.org/10.1016/j.physletb.2008.07.086>. arXiv:0803.2224
12. D.V. Bugg, An explanation of Belle states $Z_b(10610)$ and $Z_b(10650)$. EPL **96**, 11002 (2011). <https://doi.org/10.1209/0295-5075/96/11002>. arXiv:1105.5492
13. P. Pakhlov, T. Ugllov, Charged charmonium-like $Z^+(4430)$ from rescattering in conventional B decays. Phys. Lett. B **748**, 183 (2015). <https://doi.org/10.1016/j.physletb.2015.06.074>. arXiv:1408.5295
14. BESIII Collaboration, M. Ablikim et al., Observation of a charged charmoniumlike structure in $e^+e^- \rightarrow \pi^+\pi^- J/\psi$ at $\sqrt{s} = 4.26$ GeV. Phys. Rev. Lett. **110**, 252001 (2013). <https://doi.org/10.1103/PhysRevLett.110.252001>. arXiv:1303.5949
15. Belle Collaboration, Z.Q. Liu et al., Study of $e^+e^- \rightarrow \pi^+\pi^- J/\psi$ and observation of a charged charmoniumlike state at Belle. Phys. Rev. Lett. **110**, 252002 (2013). <https://doi.org/10.1103/PhysRevLett.110.252002>. Erratum, *ibid.* **111** (2013) 019901, 10.1103/PhysRevLett.111.019901. arXiv:1304.0121
16. T. Xiao, S. Dobbs, A. Tomaradze, K.K. Seth, Observation of the charged hadron $Z_c^\pm(3900)$ and evidence for the neutral $Z_c^0(3900)$ in $e^+e^- \rightarrow \pi\pi J/\psi$ at $\sqrt{s} = 4170$ MeV. Phys. Lett. B **727**, 366 (2013). <https://doi.org/10.1016/j.physletb.2013.10.041>. arXiv:1304.3036
17. M.B. Voloshin, $Z_c(3900)$ -what is inside? Phys. Rev. D **87**, 091501 (2013). <https://doi.org/10.1103/PhysRevD.87.091501>. arXiv:1304.0380
18. E. Braaten, How the $Z_c(3900)$ reveals the spectra of charmonium hybrids and tetraquarks. Phys. Rev. Lett. **111**, 162003 (2013). <https://doi.org/10.1103/PhysRevLett.111.162003>. arXiv:1305.6905
19. R.H. Dalitz, On the analysis of τ -meson data and the nature of the τ -meson. Phil. Mag. Ser. **44**, 1068 (1953). <https://doi.org/10.1080/14786441008520365>
20. LHCb Collaboration, R. Aaij et al., Evidence for an $\eta_c(1S)\pi^-$ resonance in $B^0 \rightarrow \eta_c(1S)K^+\pi^-$ decays. Eur. Phys. J. C **78**, 1019 (2018). <https://doi.org/10.1140/epjc/s10052-018-6447-z>. arXiv:1809.07416
21. H. Sundu, S.S. Agaev, K. Azizi, New charged resonance $Z_c^-(4100)$: the spectroscopic parameters and width. Eur. Phys. J. C

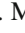

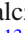


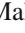
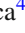

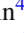



- 79, 215 (2019). <https://doi.org/10.1140/epjc/s10052-019-6737-0>. arXiv:1812.10094
22. J. Wu, X. Liu, Y.-R. Liu, S.-L. Zhu, Systematic studies of charmonium-, bottomonium-, and B_c -like tetraquark states. *Phys. Rev. D* **99**, 014037 (2019). <https://doi.org/10.1103/PhysRevD.99.014037>. arXiv:1810.06886
 23. M.B. Voloshin, $Z_c(4100)$ and $Z_c(4200)$ as hadrocharmonium. *Phys. Rev. D* **98**, 094028 (2018). <https://doi.org/10.1103/PhysRevD.98.094028>. arXiv:1810.08146
 24. Belle Collaboration, K. Chilikin et al., Observation of a new charged charmoniumlike state in $\bar{B}^0 \rightarrow J/\psi K^- \pi^+$ decays. *Phys. Rev. D* **90**, 112009 (2014). <https://doi.org/10.1103/PhysRevD.90.112009>. arXiv:1408.6457
 25. LHCb Collaboration, R. Aaij et al., Model-independent observation of exotic contributions to $B^0 \rightarrow J/\psi K^+ \pi^-$ decays. *Phys. Rev. Lett.* **122**, 152002 (2019). <https://doi.org/10.1103/PhysRevLett.122.152002>. arXiv:1901.05745
 26. X. Cao, J.-P. Dai, Spin parity of $Z_c^-(4100)$, $Z_1^+(4050)$, and $Z_2^+(4250)$. *Phys. Rev. D* **100**, 054004 (2019). <https://doi.org/10.1103/PhysRevD.100.054004>. arXiv:1811.06434
 27. Belle Collaboration, R. Mizuk et al., Observation of two resonance-like structures in the $\pi^+ \chi_{c1}$ mass distribution in exclusive $\bar{B}^0 \rightarrow K^- \pi^+ \chi_{c1}$ decays. *Phys. Rev. D* **78**, 072004 (2008). <https://doi.org/10.1103/PhysRevD.78.072004>. arXiv:0806.4098
 28. Q. Zhao, Some insights into the newly observed $Z_c(4100)$ in $B^0 \rightarrow \eta_c K^+ \pi^-$ by LHCb. arXiv:1811.05357
 29. Belle Collaboration, K. Chilikin et al., Evidence for $B^+ \rightarrow h_c K^+$ and observation of $\eta_c(2S) \rightarrow p \bar{p} \pi^+ \pi^-$. *Phys. Rev. D* **100**, 012001 (2019). <https://doi.org/10.1103/PhysRevD.100.012001>. arXiv:1903.06414
 30. LHCb Collaboration, A.A. Alves Jr. et al., The LHCb detector at the LHC. *JINST* **3**, S08005 (2008). <https://doi.org/10.1088/1748-0221/3/08/S08005>
 31. LHCb Collaboration, R. Aaij et al., LHCb detector performance. *Int. J. Mod. Phys. A* **30**, 1530022 (2015). <https://doi.org/10.1142/S0217751X15300227>. arXiv:1412.6352
 32. R. Aaij et al., Performance of the LHCb vertex locator. *JINST* **9**, P09007 (2014). <https://doi.org/10.1088/1748-0221/9/09/P09007>. arXiv:1405.7808
 33. R. Arink et al., Performance of the LHCb outer tracker. *JINST* **9**, P01002 (2014). <https://doi.org/10.1088/1748-0221/9/01/P01002>. arXiv:1311.3893
 34. P. d'Argent et al., Improved performance of the LHCb outer tracker in LHC Run 2. *JINST* **12**, P11016 (2017). <https://doi.org/10.1088/1748-0221/12/11/P11016>. arXiv:1708.00819
 35. M. Adinolfi et al., Performance of the LHCb RICH detector at the LHC. *Eur. Phys. J. C* **73**, 2431 (2013). <https://doi.org/10.1140/epjc/s10052-013-2431-9>. arXiv:1211.6759
 36. A.A. Alves Jr. et al., Performance of the LHCb muon system. *JINST* **8**, P02022 (2013). <https://doi.org/10.1088/1748-0221/8/02/P02022>. arXiv:1211.1346
 37. R. Aaij et al., The LHCb trigger and its performance in 2011. *JINST* **8**, P04022 (2013). <https://doi.org/10.1088/1748-0221/8/04/P04022>. arXiv:1211.3055
 38. V.V. Gligorov, M. Williams, Efficient, reliable and fast high-level triggering using a bonsai boosted decision tree. *JINST* **8**, P02013 (2013). <https://doi.org/10.1088/1748-0221/8/02/P02013>. arXiv:1210.6861
 39. T. Likhomanenko et al., LHCb topological trigger reoptimization. *J. Phys. Conf. Ser.* **664**, 082025 (2015). <https://doi.org/10.1088/1742-6596/664/8/082025>. arXiv:1510.00572
 40. T. Sjöstrand, S. Mrenna, P. Skands, A brief introduction to PYTHIA 8.1. *Comput. Phys. Commun.* **178**, 852 (2008). <https://doi.org/10.1016/j.cpc.2008.01.036>. arXiv:0710.3820
 41. I. Belyaev et al., Handling of the generation of primary events in Gauss, the LHCb simulation framework. *J. Phys. Conf. Ser.* **331**, 032047 (2011). <https://doi.org/10.1088/1742-6596/331/3/032047>
 42. D.J. Lange, The EvtGen particle decay simulation package. *Nucl. Instrum. Methods A* **462**, 152 (2001). [https://doi.org/10.1016/S0168-9002\(01\)00089-4](https://doi.org/10.1016/S0168-9002(01)00089-4)
 43. N. Davidson, T. Przedzinski, Z. Was, PHOTOS interface in C++: technical and physics documentation. *Comput. Phys. Commun.* **199**, 86 (2016). <https://doi.org/10.1016/j.cpc.2015.09.013>. arXiv:1011.0937
 44. Geant4 Collaboration, J. Allison et al., Geant4 developments and applications. *IEEE Trans. Nucl. Sci.* **53**, 270 (2006). <https://doi.org/10.1109/TNS.2006.869826>
 45. Geant4 Collaboration, S. Agostinelli et al., Geant4: a simulation toolkit. *Nucl. Instrum. Methods A* **506**, 250 (2003). [https://doi.org/10.1016/S0168-9002\(03\)01368-8](https://doi.org/10.1016/S0168-9002(03)01368-8)
 46. M. Clemencic et al., The LHCb simulation application, gauss: design, evolution and experience. *J. Phys. Conf. Ser.* **331**, 032023 (2011). <https://doi.org/10.1088/1742-6596/331/3/032023>
 47. D. Müller, M. Clemencic, G. Corti, M. Gersabeck, ReDecay: a novel approach to speed up the simulation at LHCb. *Eur. Phys. J. C* **78**, 1009 (2018). <https://doi.org/10.1140/epjc/s10052-018-6469-6>. arXiv:1810.10362
 48. W.D. Hulsbergen, Decay chain fitting with a Kalman filter. *Nucl. Instrum. Methods A* **552**, 566 (2005). <https://doi.org/10.1016/j.nima.2005.06.078>. arXiv:physics/0503191
 49. Particle Data Group, S. Navas et al., Review of particle physics. *Phys. Rev. D* **110**, 030001 (2024). <https://doi.org/10.1103/PhysRevD.110.030001>. <http://pdg.lbl.gov/>
 50. Y. Freund, R.E. Schapire, A decision-theoretic generalization of on-line learning and an application to boosting. *J. Comput. Syst. Sci.* **55**, 119 (1997). <https://doi.org/10.1006/jcss.1997.1504>
 51. L. Breiman, J.H. Friedman, R.A. Olshen, C.J. Stone, *Classification and Regression Trees* (Wadsworth international group, Belmont, 1984)
 52. R. Aaij et al., Selection and processing of calibration samples to measure the particle identification performance of the LHCb experiment in Run 2. *Eur. Phys. J. Tech. Instrum.* **6**, 1 (2019). <https://doi.org/10.1140/epjti/s40485-019-0050-z>. arXiv:1803.00824
 53. L. Anderlini et al., The PIDCalib package, LHCb-PUB-2016-021 (2016). http://cdsweb.cern.ch/search?p=LHCb-PUB-2016-021&f=reportnumber&action_search=Search&c=LHCb+Notes
 54. W. Verkerke, D.P. Kirkby, The RooFit toolkit for data modeling. *eConf C0303241*, MOLT007 (2003). arXiv:physics/0306116
 55. D.M. Santos, F. Dupertuis, Mass distributions marginalized over per-event errors. *Nucl. Instrum. Methods A* **764**, 150 (2014). <https://doi.org/10.1016/j.nima.2014.06.081>. arXiv:1312.5000
 56. T. Skwarnicki, A study of the radiative cascade transitions between the Upsilon-prime and Upsilon resonances. PhD thesis, Institute of Nuclear Physics, Krakow (1986). DESY-F31-86-02
 57. M. Pivk, F.R. Le Diberder, sPlot: a statistical tool to unfold data distributions. *Nucl. Instrum. Methods A* **555**, 356 (2005). <https://doi.org/10.1016/j.nima.2005.08.106>. arXiv:physics/0402083
 58. J. Back et al., Laura⁺⁺: a Dalitz plot fitter. *Comput. Phys. Commun.* **231**, 198 (2018). <https://doi.org/10.1016/j.cpc.2018.04.017>. arXiv:1711.09854
 59. E. Ben-Haim, R. Brun, B. Echenard, T.E. Latham, JFIT: a framework to obtain combined experimental results through joint fits. arXiv:1409.5080
 60. D.J. Herndon, P. Söding, R.J. Cashmore, Generalized isobar model formalism. *Phys. Rev. D* **11**, 3165 (1975). <https://doi.org/10.1103/PhysRevD.11.3165>
 61. D. Morgan, Phenomenological analysis of $I = \frac{1}{2}$ single-pion production processes in the energy range 500 to 700 MeV. *Phys. Rev.* **166**, 1731 (1968). <https://doi.org/10.1103/PhysRev.166.1731>

65. F. James, *Statistical Methods in Experimental Physics* (World Scientific Publishing, Singapore, 2006)
66. LHCb Collaboration, R. Aaij et al., Amplitude analysis of $B^0 \rightarrow \bar{D}^0 D_s^+ \pi^-$ and $B^+ \rightarrow D^- D_s^+ \pi^+$ decays. *Phys. Rev. D* **108**, 012017 (2023). <https://doi.org/10.1103/PhysRevD.108.012017>. arXiv:2212.02717
67. LHCb Collaboration, R. Aaij et al., Evidence of a $J/\psi K_S^0$ structure in $B^0 \rightarrow J/\psi \phi K_S^0$ decays. *Phys. Rev. Lett.* **131**, 131901 (2023). <https://doi.org/10.1103/PhysRevLett.131.131901>. arXiv:2301.04899
68. LHCb Collaboration, R. Aaij et al., Observation of the resonant character of the $Z(4430)^-$ state. *Phys. Rev. Lett.* **112**, 222002 (2014). <https://doi.org/10.1103/PhysRevLett.112.222002>. arXiv:1404.1903

LHCb Collaboration

R. Aaij³⁸, A.S.W. Abdelmotteleb⁵⁷, C. Abellan Beteta⁵¹, F. Abudinén⁵⁷, T. Ackernley⁶¹, A. A. Adefisoye⁶⁹, B. Adeva⁴⁷, M. Adinolfi⁵⁵, P. Adlarson⁸⁵, C. Agapopoulou¹⁴, C. A. Aidala⁸⁷, Z. Ajaltouni¹¹, S. Akar¹¹, K. Akiba³⁸, P. Albicocco²⁸, J. Albrecht^{19,g}, R. Aleksiejunas⁸⁰, F. Alessio⁴⁹, P. Alvarez Cartelle⁵⁶, R. Amalric¹⁶, S. Amato³, J. L. Amey⁵⁵, Y. Amhis¹⁴, L. An⁶, L. Anderlini²⁷, M. Andersson⁵¹, P. Andreola⁵¹, M. Andreotti²⁶, S. Andres Estrada⁸⁴, A. Anelli^{31,p,49}, D. Ao⁷, C. Arata¹², F. Archilli^{37,w}, Z. Areg⁶⁹, M. Argenton²⁶, S. Arguedas Cuendis^{9,49}, L. Arnone^{31,p}, A. Artamonov⁴⁴, M. Artuso⁶⁹, E. Aslanides¹³, R. Ataíde Da Silva⁵⁰, M. Atzeni⁶⁵, B. Audurier¹², J. A. Authier¹⁵, D. Bacher⁶⁴, I. Bachiller Perea⁵⁰, S. Bachmann²², M. Bachmayer⁵⁰, J. J. Back⁵⁷, P. Baladron Rodriguez⁴⁷, V. Balagura¹⁵, A. Balboni²⁶, W. Baldini²⁶, Z. Baldwin⁷⁸, L. Balzani¹⁹, H. Bao⁷, J. Baptista de Souza Leite², C. Barbero Pretel^{12,47}, M. Barbetti²⁷, I. R. Barbosa⁷⁰, R. J. Barlow⁶³, M. Barnyakov²⁵, S. Barsuk¹⁴, W. Barter⁵⁹, J. Bartz⁶⁹, S. Bashir⁴⁰, B. Batsukh⁵, P. B. Battista¹⁴, A. Bay⁵⁰, A. Beck⁶⁵, M. Becker¹⁹, F. Bedeschi³⁵, I. B. Bediaga², N. A. Behling¹⁹, S. Belin⁴⁷, A. Bellavista²⁵, K. Belous⁴⁴, I. Belov²⁹, I. Belyaev³⁶, G. Benane¹³, G. Bencivenni²⁸, E. Ben-Haim¹⁶, A. Berezhnoy⁴⁴, R. Bernet⁵¹, S. Bernet Andres⁴⁶, A. Bertolin³³, C. Betancourt⁵¹, F. Betti⁵⁹, J. Bex⁵⁶, Ia. Bezshyiko⁵¹, O. Bezshyyko⁸⁶, J. Bhom⁴¹, M. S. Bieker¹⁸, N. V. Biesuz²⁶, P. Billoir¹⁶, A. Biolchini³⁸, M. Birch⁶², F. C. R. Bishop¹⁰, A. Bitadze⁶³, A. Bizzetti^{27,q}, T. Blake^{57,c}, F. Blanc⁵⁰, J. E. Blank¹⁹, S. Blusk⁶⁹, V. Bocharnikov⁴⁴, J. A. Boelhave¹⁹, O. Boente Garcia¹⁵, T. Boettcher⁶⁸, A. Bohare⁵⁹, A. Boldyrev⁴⁴, C. S. Bolognani⁸², R. Bolzonella^{26,m}, R. B. Bonacci¹, N. Bondar^{44,49}, A. Bordelius⁴⁹, F. Borgato^{33,49}, S. Borghi⁶³, M. Borsato^{31,p}, J. T. Borsuk⁸³, E. Bottalico⁶¹, S. A. Bouchiba⁵⁰, M. Bovill⁶⁴, T. J. V. Bowcock⁶¹, A. Boyer⁴⁹, C. Bozzi²⁶, J. D. Brandenburg⁸⁸, A. Brea Rodriguez⁵⁰, N. Breer¹⁹, J. Brodzicka⁴¹, A. Brossa Gonzalo^{47,*}, J. Brown⁶¹, D. Brundu³², E. Buchanan⁵⁹, M. Burgos Marcos⁸², A. T. Burke⁶³, C. Burr⁴⁹, C. Buti²⁷, J. S. Butter⁵⁶, J. Buytaert⁴⁹, W. Byczynski⁴⁹, S. Cadeddu³², H. Cai⁷⁵, Y. Cai⁵, A. Caillet¹⁶, R. Calabrese^{26,m}, S. Calderon Ramirez⁹, L. Calefice⁴⁵, S. Cali²⁸, M. Calvi^{31,p}, M. Calvo Gomez⁴⁶, P. Camargo Magalhaes^{2,a}, J. I. Cambon Bouzas⁴⁷, P. Campana²⁸, D. H. Campora Perez⁸², A. F. Campoverde Quezada⁷, S. Capelli³¹, M. Caporale²⁵, L. Capriotti²⁶, R. Caravaca-Mora⁹, A. Carbone^{25,k}, L. Carcedo Salgado⁴⁷, R. Cardinale^{29,n}, A. Cardini³², P. Carniti³¹, L. Carus²², A. Casais Vidal⁶⁵, R. Caspary²², G. Casse⁶¹, M. Cattaneo⁴⁹, G. Cavallero²⁶, V. Cavallini^{26,m}, S. Celani²², I. Celestino^{35,t}, S. Cesare^{30,o}, F. Cesario Laterza Lopes², A. J. Chadwick⁶¹, I. Chahrouh⁸⁷, H. Chang^{4,d}, M. Charles¹⁶, Ph. Charpentier⁴⁹, E. Chatzianagnostou³⁸, R. Cheaib⁷⁹, M. Chefdeville¹⁰, C. Chen⁵⁶, J. Chen⁵⁰, S. Chen⁵, Z. Chen⁷, M. Cherif¹², A. Chernov⁴¹, S. Chernyshenko⁵³, X. Chiotopoulos⁸², V. Chobanova⁸⁴, M. Chruszcz⁴¹, A. Chubykin⁴⁴, V. Chulikov^{28,36,49}, P. Ciambone²⁸, X. Cid Vidal⁴⁷, G. Ciezarek⁴⁹, P. Cifra³⁸, P. E. L. Clarke⁵⁹, M. Clemencic⁴⁹, H. V. Cliff⁵⁶, J. Closier⁴⁹, C. Cocha Toapaxi²², V. Coco⁴⁹, J. Cogan¹³, E. Cogneras¹¹, L. Cojocariu⁴³, S. Collaviti⁵⁰, P. Collins⁴⁹, T. Colombo⁴⁹, M. Colonna¹⁹, A. Comerma-Montells⁴⁵, L. Congedo²⁴, J. Connaughton⁵⁷, A. Contu³², N. Cooke⁶⁰, G. Cordova^{35,t}, C. Coronel⁶⁶, I. Corredoira¹², A. Correia¹⁶, G. Corti⁴⁹, J. Cottee Meldrum⁵⁵, B. Couturier⁴⁹, D. C. Craik⁵¹, M. Cruz Torres^{2,h}, E. Curras Rivera⁵⁰, R. Currie⁵⁹, C. L. Da Silva⁶⁸, S. Dadabaev⁴⁴, L. Dai⁷², X. Dai⁴, E. Dall'Occo⁴⁹, J. Dalseno⁸⁴, C. D'Ambrosio⁶², J. Daniel¹¹, P. d'Argent²⁴, G. Darze³, A. Davidson⁵⁷, J. E. Davies⁶³, O. De Aguiar Francisco⁶³, C. De Angelis^{32,l}, F. De Benedetti⁴⁹, J. de Boer³⁸, K. De Bruyn⁸¹, S. De Capua⁶³, M. De Cian⁶³, U. De Freitas Carneiro Da Graca^{2,b}, E. De Lucia²⁸, J. M. De Miranda², L. De Paula³, M. De Serio^{24,i}, P. De Simone²⁸, F. De Vellis¹⁹, J. A. de Vries⁸², F. Debernardis²⁴, D. Decamp¹⁰, S. Dekkers¹, L. Del Buono¹⁶, B. Delaney⁶⁵, H.-P. Dembinski¹⁹, J. Deng⁸, V. Denysenko⁵¹, O. Deschamps¹¹, F. Dettori^{32,l}, B. Dey⁷⁹, P. Di Nezza²⁸, I. Diachkov⁴⁴, S. Didenko⁴⁴, S. Ding⁶⁹,

Y. Ding⁵⁰, L. Dittmann²², V. Dobishuk⁵³, A. D. Docheva⁶⁰, A. Doheny⁵⁷, C. Dong^{4,d}, A. M. Donohoe²³, F. Dordei³², A. C. dos Reis², A. D. Dowling⁶⁹, L. Dreyfus¹³, W. Duan⁷³, P. Duda⁸³, L. Dufour⁴⁹, V. Duk³⁴, P. Durante⁴⁹, M. M. Duras⁸³, J. M. Durham⁶⁸, O. D. Durmus⁷⁹, A. Dziurda⁴¹, A. Dzyuba⁴⁴, S. Easo⁵⁸, E. Eckstein¹⁸, U. Egede¹, A. Egorychev⁴⁴, V. Egorychev⁴⁴, S. Eisenhardt⁵⁹, E. Ejopu⁶¹, L. Eklund⁸⁵, M. Elashri⁶⁶, J. Ellbracht¹⁹, S. Ely⁶², A. Ene⁴³, J. Eschle⁶⁹, S. Esen²², T. Evans³⁸, F. Fabiano³², S. Faghini⁶⁶, L. N. Falcao², B. Fang⁷, R. Fantechi³⁵, L. Fantini^{34,s}, M. Faria⁵⁰, K. Farmer⁵⁹, D. Fazzini^{31,p}, L. Felkowski⁸³, M. Feng^{5,7}, M. Feo¹⁹, A. Fernandez Casani⁴⁸, M. Fernandez Gomez⁴⁷, A. D. Fernez⁶⁷, F. Ferrari^{25,k}, F. Ferreira Rodrigues³, M. Ferrillo⁵¹, M. Ferro-Luzzi⁴⁹, S. Filippov⁴⁴, R. A. Fini²⁴, M. Fiorini^{26,m}, M. Firlej⁴⁰, K. L. Fischer⁶⁴, D. S. Fitzgerald⁸⁷, C. Fitzpatrick⁶³, T. Fiutowski⁴⁰, F. Fleuret¹⁵, A. Fomin⁵², M. Fontana²⁵, L. F. Foreman⁶³, R. Forty⁴⁹, D. Foulds-Holt⁵⁹, V. Franco Lima³, M. Franco Sevilla⁶⁷, M. Frank⁴⁹, E. Franzoso^{26,m}, G. Frau⁶³, C. Frei⁴⁹, D. A. Friday^{49,63}, J. Fu⁷, Q. Fühling^{19,g,56}, T. Fulghesu¹³, G. Galati²⁴, M. D. Galati³⁸, A. Gallas Torreira⁴⁷, D. Galli^{25,k}, S. Gambetta⁵⁹, M. Gandelman³, P. Gandini³⁰, B. Ganie⁶³, H. Gao⁷, R. Gao⁶⁴, T. Q. Gao⁵⁶, Y. Gao⁸, Y. Gao⁶, Y. Gao⁸, L.M. Garcia Martin⁵⁰, P. Garcia Moreno⁴⁵, J. García Pardiñas⁶⁵, P. Gardner⁶⁷, K. G. Garg⁸, L. Garrido⁴⁵, C. Gaspar⁴⁹, A. Gavrikov³³, L. L. Gerken¹⁹, E. Gersabeck²⁰, M. Gersabeck²⁰, T. Gershon⁵⁷, S. Ghizzo^{29,n}, Z. Ghorbanimoghaddam⁵⁵, L. Giambastiani^{33,r}, F. I. Giasemis^{16,f}, V. Gibson⁵⁶, H. K. Gienza⁴², A. L. Gilman⁶⁴, M. Giovannetti²⁸, A. Gioventù⁴⁵, L. Girardey^{58,63}, M. A. Giza⁴¹, F. C. Glaser^{14,22}, V. V. Gligorov¹⁶, C. Göbel⁷⁰, L. Golinka-Bezshyyko⁸⁶, E. Golobardes⁴⁶, D. Golubkov⁴⁴, A. Golutvin^{49,62}, S. Gomez Fernandez⁴⁵, W. Gomulka⁴⁰, I. Gonçalves Vaz⁴⁹, F. Goncalves Abrantes⁶⁴, M. Goncerz⁴¹, G. Gong^{4,d}, J. A. Gooding¹⁹, I. V. Gorelov⁴⁴, C. Gotti³¹, E. Govorkova⁶⁵, J. P. Grabowski¹⁸, L. A. Granado Cardoso⁴⁹, E. Graugés⁴⁵, E. Graverini^{50,u}, L. Grazette⁵⁷, G. Graziani²⁷, A. T. Grecu⁴³, L. M. Greeven³⁸, N. A. Grieser⁶⁶, L. Grillo⁶⁰, S. Gromov⁴⁴, C. Gu¹⁵, M. Guarise²⁶, L. Guerry¹¹, V. Guliaeva⁴⁴, P. A. Günther²², A.-K. Guseinov⁵⁰, E. Gushchin⁴⁴, Y. Guz^{6,49}, T. Gys⁴⁹, K. Habermann¹⁸, T. Hadavizadeh¹, C. Hadjivasiliou⁶⁷, G. Haefeli⁵⁰, C. Haen⁴⁹, S. Haken⁵⁶, G. Hallett⁵⁷, P. M. Hamilton⁶⁷, J. Hammerich⁶¹, Q. Han³³, X. Han^{22,49}, S. Hansmann-Menzemer²², L. Hao⁷, N. Harnew⁶⁴, T. H. Harris¹, M. Hartmann¹⁴, S. Hashmi⁴⁰, J. He^{7,e}, A. Hedes⁶³, F. Hemmer⁴⁹, C. Henderson⁶⁶, R. Henderson¹⁴, R.D.L. Henderson¹, A.M. Hennequin⁴⁹, K. Hennessy⁶¹, L. Henry⁵⁰, J. Herd⁶², P. Herrero Gascon²², J. Heuel¹⁷, A. Hicheur³, G. Hijano Mendizabal⁵¹, J. Horswill⁶³, R. Hou⁸, Y. Hou¹¹, D. C. Houston⁶⁰, N. Howarth⁶¹, J. Hu⁷³, W. Hu⁷, X. Hu^{4,d}, W. Hulsbergen³⁸, R. J. Hunter⁵⁷, M. Hushchyn⁴⁴, D. Hutchcroft⁶¹, M. Idzik⁴⁰, D. Ilin⁴⁴, P. Ilten⁶⁶, A. Iniukhin⁴⁴, A. Iohner¹⁰, A. Ishteev⁴⁴, K. Ivshin⁴⁴, H. Jage¹⁷, S. J. Jaimes Elles^{48,49,77}, S. Jakobsen⁴⁹, E. Jans³⁸, B. K. Jashal⁴⁸, A. Jawahery⁶⁷, C. Jayaweera⁵⁴, V. Jevtic¹⁹, Z. Jia¹⁶, E. Jiang⁶⁷, X. Jiang^{5,7}, Y. Jiang⁷, Y. J. Jiang⁶, E. Jimenez Moya⁹, N. Jindal⁸⁸, M. John⁶⁴, A. John Rubesh Rajan²³, D. Johnson⁵⁴, C. R. Jones⁵⁶, S. Joshi⁴², B. Jost⁴⁹, J. Juan Castella⁵⁶, N. Jurik⁴⁹, I. Juszczak⁴¹, D. Kaminaris⁵⁰, S. Kandybei⁵², M. Kane⁵⁹, Y. Kang^{4,d}, C. Kar¹¹, M. Karacson⁴⁹, A. Kauniskangas⁵⁰, J. W. Kautz⁶⁶, M. K. Kazanecki⁴¹, F. Keizer⁴⁹, M. Kenzie⁵⁶, T. Ketel³⁸, B. Khanji⁶⁹, A. Kharisova⁴⁴, S. Kholodenko^{49,62}, G. Khreich¹⁴, T. Kirn¹⁷, V. S. Kirsebom^{31,p}, O. Kitouni⁶⁵, S. Klaver³⁹, N. Kleijne^{35,t}, D. K. Klekots⁸⁶, K. Klimaszewski⁴², M. R. Kmiec⁴², T. Knospe¹⁹, S. Koliiev⁵³, L. Kolk¹⁹, A. Konoplyannikov⁶, P. Kopciwicz⁴⁹, P. Koppenburg³⁸, A. Korchin⁵², M. Korolev⁴⁴, I. Kostiuik³⁸, O. Kot⁵³, S. Kotriakhova⁴⁴, E. Kowalczyk⁶⁷, A. Kozachuk⁴⁴, P. Kravchenko⁴⁴, L. Kravchuk⁴⁴, O. Kravcov⁸⁰, M. Kreps⁵⁷, P. Krokovny⁴⁴, W. Krupa⁶⁹, W. Krzemien⁴², O. Kshyvanskyi⁵³, S. Kubis⁸³, M. Kucharczyk⁴¹, V. Kudryavtsev⁴⁴, E. Kulikova⁴⁴, A. Kupsc⁸⁵, V. Kushnir⁵², B. Kutsenko¹³, J. Kvapil⁶⁸, I. Kyryllin⁵², D. Lacarrere⁴⁹, P. Laguarda Gonzalez⁴⁵, A. Lai³², A. Lampis³², D. Lancierini⁶², C. Landesa Gomez⁴⁷, J. J. Lane¹, G. Lanfranchi²⁸, C. Langenbruch²², J. Langer¹⁹, O. Lantwin⁴⁴, T. Latham⁵⁷, F. Lazzari^{35,u,49}, C. Lazzeroni⁵⁴, R. Le Gac¹³, H. Lee⁶¹, R. Lefèvre¹¹, A. Leflat⁴⁴, S. Legotin⁴⁴, M. Lehuraux⁵⁷, E. Lemos Cid⁴⁹, O. Leroy¹³, T. Lesiak⁴¹, E. D. Lesser⁴⁹, B. Leverington²², A. Li^{4,d}, C. Li⁴, C. Li¹³, H. Li⁷³, J. Li⁸, K. Li⁷⁶, L. Li⁶³, M. Li⁸, P. Li⁷, P.-R. Li⁷⁴, Q. Li^{5,7}, T. Li⁷², T. Li⁷³, Y. Li⁸, Y. Li⁵, Y. Li⁴, Z. Lian^{4,d}, Q. Liang⁸, X. Liang⁶⁹, Z. Liang³², S. Libralon⁴⁸, A. L. Lightbody¹², C. Lin⁷, T. Lin⁵⁸, R. Lindner⁴⁹, H. Linton⁶², R. Litvinov³², D. Liu⁸, F. L. Liu¹, G. Liu⁷³, K. Liu⁷⁴, S. Liu^{5,7}, W. Liu⁸, Y. Liu⁵⁹, Y. Liu⁷⁴, Y. L. Liu⁶², G. Loachamin Ordonez⁷⁰, A. Lobo Salvia⁴⁵, A. Loi³², T. Long⁵⁶, J. H. Lopes³, A. Lopez Huertas⁴⁵, C. Lopez Iribarnegaray⁴⁷, S. L.ópez Soliño⁴⁷, Q. Lu¹⁵, C. Lucarelli⁴⁹, D. Lucchesi^{33,r}, M. Lucio Martinez⁴⁸, Y. Luo⁶, A. Lupato^{33,j}, E. Luppi^{26,m}, K. Lynch²³, X.-R. Lyu⁷, G. M. Ma^{4,d}, S. Maccolini¹⁹, F. Machefert¹⁴, F. Maciuc⁴³, B. Mack⁶⁹, I. Mackay⁶⁴, L. M. Mackey⁶⁹, L. R. Madhan Mohan⁵⁶, M. J. Madurai⁵⁴, D. Magdalinski³⁸

D. Maisuzenko⁴⁴, J. J. Malczewski⁴¹, S. Malde⁶⁴, L. Malentacca⁴⁹, A. Malinin⁴⁴, T. Maltsev⁴⁴, G. Manca^{32,l}, G. Mancinelli¹³, C. Mancuso¹⁴, R. Manera Escalero⁴⁵, F. M. Manganella³⁷, D. Manuzzi²⁵, D. Marangotto^{30,o}, J. F. Marchand¹⁰, R. Marchevski⁵⁰, U. Marconi²⁵, E. Mariani¹⁶, S. Mariani⁴⁹, C. Marin Benito⁴⁵, J. Marks²², A. M. Marshall⁵⁵, L. Martel⁶⁴, G. Martelli³⁴, G. Martellotti³⁶, L. Martinazzoli⁴⁹, M. Martinelli^{31,p}, D. Martinez Gomez⁸¹, D. Martinez Santos⁸⁴, F. Martinez Vidal⁴⁸, A. Martorell i Granollers⁴⁶, A. Massafferri², R. Matev⁴⁹, A. Mathad⁴⁹, V. Matiunin⁴⁴, C. Matteuzzi⁶⁹, K. R. Mattioli¹⁵, A. Mauri⁶², E. Maurice¹⁵, J. Mauricio⁴⁵, P. Mayencourt⁵⁰, J. Mazorra de Cos⁴⁸, M. Mazurek⁴², M. McCann⁶², T. H. McGrath⁶³, N. T. McHugh⁶⁰, A. McNab⁶³, R. McNulty²³, B. Meadows⁶⁶, G. Meier¹⁹, D. Melnychuk⁴², D. Mendoza Granada¹⁶, P. Menendez Valdes Perez⁴⁷, F. M. Meng^{4,d}, M. Merk^{38,82}, A. Merli^{30,50}, L. Meyer Garcia⁶⁷, D. Miao^{5,7}, H. Miao⁷, M. Mikhasenko⁷⁸, D. A. Milanés^{77,z}, A. Minotti^{31,p}, E. Minucci²⁸, T. Miralles¹¹, B. Mitreska¹⁹, D. S. Mitzel¹⁹, A. Modak⁵⁸, L. Moeser¹⁹, R. D. Moise¹⁷, E. F. Molina Cardenas⁸⁷, T. Mombächer⁴⁹, M. Monk^{1,57}, S. Monteil¹¹, A. Morcillo Gomez⁴⁷, G. Morello²⁸, M. J. Morello^{35,t}, M. P. Morgenthaler²², A. Moro^{31,p}, J. Moron⁴⁰, W. Morren³⁸, A. B. Morris⁴⁹, A. G. Morris¹³, R. Mountain⁶⁹, H. Mu^{4,d}, Z. M. Mu⁶, E. Muhammad⁵⁷, F. Muheim⁵⁹, M. Mulder⁸¹, K. Müller⁵¹, F. Muñoz-Rojas⁹, R. Murta⁶², V. Mytrochenko⁵², P. Naik⁶¹, T. Nakada⁵⁰, R. Nandakumar⁵⁸, T. Nanut⁴⁹, I. Nasteva³, M. Needham⁵⁹, E. Nekrasova⁴⁴, N. Neri^{30,o}, S. Neubert¹⁸, N. Neufeld⁴⁹, P. Neustroev⁴⁴, J. Nicolini⁴⁹, D. Nicotra⁸², E. M. Niel¹⁵, N. Nikitin⁴⁴, L. Nisi¹⁹, Q. Niu⁷⁴, P. Nogarolli³, P. Nogga¹⁸, C. Normand⁵⁵, J. Novoa Fernandez⁴⁷, G. Nowak⁶⁶, C. Nunez⁸⁷, H. N. Nur⁶⁰, A. Oblakowska-Mucha⁴⁰, V. Obraztsov⁴⁴, T. Oeser¹⁷, A. Okhotnikov⁴⁴, O. Okhrimenko⁵³, R. Oldeman^{32,l}, F. Oliva^{49,59}, E. Olivart Pino⁴⁵, M. Olocco¹⁹, C. J. G. Onderwater⁸², R. H. O'Neil⁴⁹, J. S. Ordonez Soto¹¹, D. Osthues¹⁹, J. M. Otalora Goicochea³, P. Owen⁵¹, A. Oyanguren⁴⁸, O. Ozcelik⁴⁹, F. Paciolla^{35,x}, A. Padee⁴², K. O. Padeken¹⁸, B. Pagare⁴⁷, T. Pajero⁴⁹, A. Palano²⁴, M. Palutan²⁸, C. Pan⁷⁵, X. Pan^{4,d}, S. Panebianco¹², G. Panshin⁵, L. Paolucci⁶³, A. Papanestis⁵⁸, M. Pappagallo^{24,i}, L. L. Pappalardo²⁶, C. Pappenheimer⁶⁶, C. Parkes⁶³, D. Parmar⁷⁸, B. Passalacqua^{26,m}, G. Passaleva²⁷, D. Passaro^{35,t,49}, A. Pastore²⁴, M. Patel⁶², J. Patoc⁶⁴, C. Patrignani^{25,k}, A. Paul⁶⁹, C. J. Pawley⁸², A. Pellegrino³⁸, J. Peng^{5,7}, X. Peng⁷⁴, M. Pepe Altarelli²⁸, S. Perazzini²⁵, D. Pereima⁴⁴, H. Pereira Da Costa⁶⁸, M. Pereira Martinez⁴⁷, A. Pereiro Castro⁴⁷, C. Perez⁴⁶, P. Perret¹¹, A. Perrevoort⁸¹, A. Perro^{13,49}, M. J. Peters⁶⁶, K. Petridis⁵⁵, A. Petrolini^{29,n}, S. Pezzulo^{29,n}, J. P. Pfaller⁶⁶, H. Pham⁶⁹, L. Pica^{35,t}, M. Piccini³⁴, L. Piccolo³², B. Pietrzyk¹⁰, G. Pietrzyk¹⁴, R. N. Pilato⁶¹, D. Pinci³⁶, F. Pisani⁴⁹, M. Pizzichemi^{31,p,49}, V. M. Placinta⁴³, M. Plo Casaus⁴⁷, T. Poeschl⁴⁹, F. Polci¹⁶, M. Poli Lener²⁸, A. Poluektov¹³, N. Polukhina⁴⁴, I. Polyakov⁶³, E. Polycarpo³, S. Ponce⁴⁹, D. Popov^{7,49}, S. Poslavskii⁴⁴, K. Prasanth⁵⁹, C. Prouve⁸⁴, D. Provenzano^{32,l,49}, V. Pugatch⁵³, G. Punzi^{35,u}, J. R. Pybus⁶⁸, S. Qasim⁵¹, Q. Q. Qian⁶, W. Qian⁷, N. Qin^{4,d}, S. Qu^{4,d}, R. Quagliani⁴⁹, R. I. Rabadan Trejo⁵⁷, R. Racz⁸⁰, J. H. Rademacker⁵⁵, M. Rama³⁵, M. Ramírez García⁸⁷, V. Ramos De Oliveira⁷⁰, M. Ramos Pernas⁵⁷, M. S. Rangel³, F. Ratnikov⁴⁴, G. Raven³⁹, M. Rebollo De Miguel⁴⁸, F. Redi^{30,j}, J. Reich⁵⁵, F. Reiss²⁰, Z. Ren⁷, P. K. Resmi⁶⁴, M. Ribalda Galvez⁴⁵, R. Ribatti⁵⁰, G. Ricart^{12,15}, D. Riccardi^{35,t}, S. Ricciardi⁵⁸, K. Richardson⁶⁵, M. Richardson-Slipper⁵⁶, K. Rinnert⁶¹, P. Robbe^{14,49}, G. Robertson⁶⁰, E. Rodrigues⁶¹, A. Rodriguez Alvarez⁴⁵, E. Rodriguez Fernandez⁴⁷, J. A. Rodriguez Lopez⁷⁷, E. Rodriguez Rodriguez⁴⁹, J. Roensch¹⁹, A. Rogachev⁴⁴, A. Rogovskiy⁵⁸, D. L. Rolf¹⁹, P. Roloff⁴⁹, V. Romanovskiy⁶⁶, A. Romero Vidal⁴⁷, G. Romolini^{26,49}, F. Ronchetti⁵⁰, T. Rong⁶, M. Rotondo²⁸, S. R. Roy²², M. S. Rudolph⁶⁹, M. Ruiz Diaz²², R. A. Ruiz Fernandez⁴⁷, J. Ruiz Vidal⁸², J. J. Saavedra-Arias⁹, J. J. Saborido Silva⁴⁷, S. E. R. Sacha Emile R.⁴⁹, N. Sagidova⁴⁴, D. Sahoo⁷⁹, N. Sahoo⁵⁴, B. Saitta^{32,l}, M. Salomoni^{31,49,p}, I. Sanderswood⁴⁸, R. Santacesaria³⁶, C. Santamarina Rios⁴⁷, M. Santimaria²⁸, L. Santoro², E. Santovetti³⁷, A. Saputi^{26,49}, D. Saranin⁴⁴, A. Sarnatskiy⁸¹, G. Sarpis⁴⁹, M. Sarpis⁸⁰, C. Satriano^{36,v}, A. Satta³⁷, M. Saur⁷⁴, D. Savrina⁴⁴, H. Sazak¹⁷, F. Sborzacchi^{28,49}, A. Scarabotto¹⁹, S. Schael¹⁷, S. Scherl⁶¹, M. Schiller²², H. Schindler⁴⁹, M. Schmelling²¹, B. Schmidt⁴⁹, N. Schmidt⁶⁸, S. Schmitt¹⁷, H.

L. Soares Lavra⁵⁹ , M.D. Sokoloff⁶⁶ , F. J. P. Soler⁶⁰ , A. Solomin⁵⁵ , A. Solovov⁴⁴ , K. Solovieva²⁰ , N. S. Sommerfeld¹⁸ , R. Song¹ , Y. Song⁵⁰ , Y. Song^{4,d} , Y. S. Song⁶ , F. L. Souza De Almeida⁶⁹ , B. Souza De Paula³ , K. M. Sowa⁴⁰ , E. Spadaro Norella^{29,n} , E. Spedicato²⁵ , J. G. Speer¹⁹ , P. Spradlin⁶⁰ , V. Sriskaran⁴⁹ , F. Stagni⁴⁹ , M. Stahl⁷⁸ , S. Stahl⁴⁹ , S. Stanislaus⁶⁴ , M. Stefaniak⁸⁸ , E. N. Stein⁴⁹ , O. Steinkamp⁵¹ , H. Stevens¹⁹ , D. Strelakina⁴⁴ , Y. Su⁷ , F. Suljik⁶⁴ , J. Sun³² , J. Sun⁶³ , L. Sun⁷⁵ , D. Sundfeld² , W. Sutcliffe⁵¹ , V. Svintozelskiy⁴⁸ , K. Swientek⁴⁰ , F. Swystun⁵⁶ , A. Szabelski⁴² , T. Szumlak⁴⁰ , Y. Tan^{4,d} , Y. Tang⁷⁵ , Y. T. Tang⁷ , M. D. Tat²² , J. A. Teixeira Jimenez⁴⁷ , A. Terentev⁴⁴ , F. Terzuoli^{35,x} , F. Teubert⁴⁹ , E. Thomas⁴⁹ , D. J. D. Thompson⁵⁴ , A. R. Thomson-Strong⁵⁹ , H. Tilquin⁶² , V. Tisserand¹¹ , S. T'Jampens¹⁰ , M. Tobin^{5,49} , T. T. Todorov²⁰ , L. Tomassetti^{26,m} , G. Tonani³⁰ , X. Tong⁶ , T. Tork³⁰ , D. Torres Machado² , L. Toscano¹⁹ , D. Y. Tou^{4,d} , C. Trippi⁴⁶ , G. Tuci²² , N. Tuning³⁸ , L. H. Uecker²² , A. Ukleja⁴⁰ , D. J. Unverzagt²² , A. Upadhyay⁴⁹ , B. Urbach⁵⁹ , A. Usachov³⁹ , A. Ustyuzhanin⁴⁴ , U. Uwer²² , V. Vagnoni²⁵ , V. Valcarce Cadenas⁴⁷ , G. Valenti²⁵ , N. Valls Canudas⁴⁹ , J. van Eldik⁴⁹ , H. Van Hecke⁶⁸ , E. van Herwijnen⁶² , C. B. Van Hulse^{47,aa} , R. Van Laak⁵⁰ , M. van Veghel³⁸ , G. Vasquez⁵¹ , R. Vazquez Gomez⁴⁵ , P. Vazquez Regueiro⁴⁷ , C. Vázquez Sierra⁸⁴ , S. Vecchi²⁶ , J. Velilla Serna⁴⁸ , J. J. Velthuis⁵⁵ , M. Veltri^{27,y} , A. Venkateswaran⁵⁰ , M. Verdognia³² , M. Vesterinen⁵⁷ , W. Vetens⁶⁹ , D. Vico Benet⁶⁴ , P. Vidrier Villalba⁴⁵ , M. Vieites Diaz^{47,49} , X. Vilasis-Cardona⁴⁶ , E. Vilella Figueras⁶¹ , A. Villa²⁵ , P. Vincent¹⁶ , B. Vivacqua³ , F. C. Volle⁵⁴ , D. vom Bruch¹³ , N. Voropaev⁴⁴ , K. Vos⁸² , C. Vrahas⁵⁹ , J. Wagner¹⁹ , J. Walsh³⁵ , E. J. Walton^{1,57} , G. Wan⁶ , A. Wang⁷ , B. Wang⁵ , C. Wang²² , G. Wang⁸ , H. Wang⁷⁴ , J. Wang⁶ , J. Wang⁵ , J. Wang^{4,d} , J. Wang⁷⁵ , M. Wang⁴⁹ , N. W. Wang⁷ , R. Wang⁵⁵ , X. Wang⁸ , X. Wang⁷³ , X. W. Wang⁶² , Y. Wang⁷⁶ , Y. Wang⁶ , Y. H. Wang⁷⁴ , Z. Wang¹⁴ , Z. Wang^{4,d} , Z. Wang³⁰ , J. A. Ward⁵⁷ , M. Waterlaet⁴⁹ , N. K. Watson⁵⁴ , D. Websdale⁶² , Y. Wei⁶ , Z. Weida⁷ , J. Wendel⁸⁴ , B. D. C. Westhenry⁵⁵ , C. White⁵⁶ , M. Whitehead⁶⁰ , E. Whiter⁵⁴ , A. R. Wiederhold⁶³ , D. Wiedner¹⁹ , M. A. Wiegertjes³⁸ , C. Wild⁶⁴ , G. Wilkinson^{49,64} , M. K. Wilkinson⁶⁶ , M. Williams⁶⁵ , M. J. Williams⁴⁹ , M. R. J. Williams⁵⁹ , R. Williams⁵⁶ , S. Williams⁵⁵ , Z. Williams⁵⁵ , F. F. Wilson⁵⁸ , M. Winn¹² , W. Wislicki⁴² , M. Witek⁴¹ , L. Witola¹⁹ , T. Wolf²² , E. Wood⁵⁶ , G. Wormser¹⁴ , S. A. Wotton⁵⁶ , H. Wu⁶⁹ , J. Wu⁸ , X. Wu⁷⁵ , Y. Wu^{6,56} , Z. Wu⁷ , K. Wyllie⁴⁹ , S. Xian⁷³ , Z. Xiang⁵ , Y. Xie⁸ , T. X. Xing³⁰ , A. Xu^{35,t} , L. Xu^{4,d} , L. Xu^{4,d} , M. Xu⁴⁹ , Z. Xu⁴⁹ , Z. Xu⁷ , Z. Xu⁵ , K. Yang⁶² , X. Yang⁶ , Y. Yang¹⁵ , Z. Yang⁶ , V. Yeroshenko¹⁴ , H. Yeung⁶³ , H. Yin⁸ , X. Yin⁷ , C. Y. Yu⁶ , J. Yu⁷² , X. Yuan⁵ , Y. Yuan^{5,7} , E. Zaffaroni⁵⁰ , J. A. Zamora Saa⁷¹ , M. Zavertyaev²¹ , M. Zdybal⁴¹ , F. Zenesini²⁵ , C. Zeng^{5,7} , M. Zeng^{4,d} , C. Zhang⁶ , D. Zhang⁸ , J. Zhang⁷ , L. Zhang^{4,d} , R. Zhang⁸ , S. Zhang⁷² , S. Zhang⁶⁴ , Y. Zhang⁶ , Y. Z. Zhang^{4,d} , Z. Zhang^{4,d} , Y. Zhao²² , A. Zhelezov²² , S. Z. Zheng⁶ , X. Z. Zheng^{4,d} , Y. Zheng⁷ , T. Zhou⁶ , X. Zhou⁸ , Y. Zhou⁷ , V. Zhovkovska⁵⁷ , L. Z. Zhu⁷ , X. Zhu^{4,d} , X. Zhu⁸ , Y. Zhu¹⁷ , V. Zhukov¹⁷ , J. Zhuo⁴⁸ , Q. Zou^{5,7} , D. Zuliani^{33,r} , G. Zunica²⁸ 

¹ School of Physics and Astronomy, Monash University, Melbourne, Australia

² Centro Brasileiro de Pesquisas Físicas (CBPF), Rio de Janeiro, Brazil

³ Universidade Federal do Rio de Janeiro (UFRJ), Rio de Janeiro, Brazil

⁴ Department of Engineering Physics, Tsinghua University, Beijing, China

⁵ Institute Of High Energy Physics (IHEP), Beijing, China

⁶ School of Physics State Key Laboratory of Nuclear Physics and Technology, Peking University, Beijing, China

⁷ University of Chinese Academy of Sciences, Beijing, China

⁸ Institute of Particle Physics, Central China Normal University, Wuhan, Hubei, China

⁹ Consejo Nacional de Rectores (CONARE), San Jose, Costa Rica

¹⁰ Université Savoie Mont Blanc, CNRS, IN2P3-LAPP, Annecy, France

¹¹ Université Clermont Auvergne, CNRS/IN2P3, LPC, Clermont-Ferrand, France

¹² Université Paris-Saclay, Centre d'Etudes de Saclay (CEA), IRFU, Saclay, France, Gif-Sur-Yvette, France

¹³ Aix Marseille Univ, CNRS/IN2P3, CPPM, Marseille, France

¹⁴ Université Paris-Saclay, CNRS/IN2P3, IJCLab, Orsay, France

¹⁵ Laboratoire Leprince-Ringuet, CNRS/IN2P3, Ecole Polytechnique, Institut Polytechnique de Paris, Palaiseau, France

¹⁶ LPNHE, Sorbonne Université, Paris Diderot Sorbonne Paris Cité, CNRS/IN2P3, Paris, France

¹⁷ I. Physikalisches Institut, RWTH Aachen University, Aachen, Germany

¹⁸ Universität Bonn - Helmholtz-Institut für Strahlen und Kernphysik, Bonn, Germany

¹⁹ Fakultät Physik, Technische Universität Dortmund, Dortmund, Germany

- 20 Physikalisches Institut, Albert-Ludwigs-Universität Freiburg, Freiburg, Germany
- 21 Max-Planck-Institut für Kernphysik (MPIK), Heidelberg, Germany
- 22 Physikalisches Institut, Ruprecht-Karls-Universität Heidelberg, Heidelberg, Germany
- 23 School of Physics, University College Dublin, Dublin, Ireland
- 24 INFN Sezione di Bari, Bari, Italy
- 25 INFN Sezione di Bologna, Bologna, Italy
- 26 INFN Sezione di Ferrara, Ferrara, Italy
- 27 INFN Sezione di Firenze, Firenze, Italy
- 28 INFN Laboratori Nazionali di Frascati, Frascati, Italy
- 29 INFN Sezione di Genova, Genoa, Italy
- 30 INFN Sezione di Milano, Milan, Italy
- 31 INFN Sezione di Milano-Bicocca, Milan, Italy
- 32 INFN Sezione di Cagliari, Monserrato, Italy
- 33 INFN Sezione di Padova, Padua, Italy
- 34 INFN Sezione di Perugia, Perugia, Italy
- 35 INFN Sezione di Pisa, Pisa, Italy
- 36 INFN Sezione di Roma La Sapienza, Rome, Italy
- 37 INFN Sezione di Roma Tor Vergata, Rome, Italy
- 38 Nikhef National Institute for Subatomic Physics, Amsterdam, The Netherlands
- 39 Nikhef National Institute for Subatomic Physics and VU University Amsterdam, Amsterdam, The Netherlands
- 40 Faculty of Physics and Applied Computer Science, AGH-University of Krakow, Kraków, Poland
- 41 Henryk Niewodniczanski Institute of Nuclear Physics Polish Academy of Sciences, Kraków, Poland
- 42 National Center for Nuclear Research (NCBJ), Warsaw, Poland
- 43 Horia Hulubei National Institute of Physics and Nuclear Engineering, Bucharest-Magurele, Romania
- 44 Authors affiliated with an Institute Formerly Covered by a Cooperation Agreement with CERN, Geneva, Switzerland
- 45 ICCUB, Universitat de Barcelona, Barcelona, Spain
- 46 La Salle, Universitat Ramon Llull, Barcelona, Spain
- 47 Instituto Galego de Física de Altas Enerxías (IGFAE), Universidade de Santiago de Compostela, Santiago de Compostela, Spain
- 48 Instituto de Física Corpuscular, Centro Mixto Universidad de Valencia-CSIC, Valencia, Spain
- 49 European Organization for Nuclear Research (CERN), Geneva, Switzerland
- 50 Institute of Physics, Ecole Polytechnique Fédérale de Lausanne (EPFL), Lausanne, Switzerland
- 51 Physik-Institut, Universität Zürich, Zürich, Switzerland
- 52 NSC Kharkiv Institute of Physics and Technology (NSC KIPT), Kharkiv, Ukraine
- 53 Institute for Nuclear Research of the National Academy of Sciences (KINR), Kyiv, Ukraine
- 54 School of Physics and Astronomy, University of Birmingham, Birmingham, UK
- 55 H.H. Wills Physics Laboratory, University of Bristol, Bristol, UK
- 56 Cavendish Laboratory, University of Cambridge, Cambridge, UK
- 57 Department of Physics, University of Warwick, Coventry, UK
- 58 STFC Rutherford Appleton Laboratory, Didcot, UK
- 59 School of Physics and Astronomy, University of Edinburgh, Edinburgh, UK
- 60 School of Physics and Astronomy, University of Glasgow, Glasgow, UK
- 61 Oliver Lodge Laboratory, University of Liverpool, Liverpool, UK
- 62 Imperial College London, London, UK
- 63 Department of Physics and Astronomy, University of Manchester, Manchester, UK
- 64 Department of Physics, University of Oxford, Oxford, UK
- 65 Massachusetts Institute of Technology, Cambridge, MA, USA
- 66 University of Cincinnati, Cincinnati, OH, USA
- 67 University of Maryland, College Park, MD, USA
- 68 Los Alamos National Laboratory (LANL), Los Alamos, NM, USA
- 69 Syracuse University, Syracuse, NY, USA
- 70 Pontifícia Universidade Católica do Rio de Janeiro (PUC-Rio), Rio de Janeiro, Brazil, associated to ³
- 71 Universidad Andres Bello, Santiago, Chile, associated to ⁵¹

- ⁷² School of Physics and Electronics, Hunan University, Changsha City, China, associated to ⁸
- ⁷³ Guangdong Provincial Key Laboratory of Nuclear Science, Guangdong-Hong Kong Joint Laboratory of Quantum Matter, Institute of Quantum Matter, South China Normal University, Guangzhou, China, associated to ⁴
- ⁷⁴ Lanzhou University, Lanzhou, China, associated to ⁵
- ⁷⁵ School of Physics and Technology, Wuhan University, Wuhan, China, associated to ⁴
- ⁷⁶ Henan Normal University, Xinxiang, China, associated to ⁸
- ⁷⁷ Departamento de Física, Universidad Nacional de Colombia, Bogota, Colombia, associated to ¹⁶
- ⁷⁸ Ruhr Universitaet Bochum, Fakultae f. Physik und Astronomie, Bochum, Germany, associated to ¹⁹
- ⁷⁹ Eotvos Lorand University, Budapest, Hungary, associated to ⁴⁹
- ⁸⁰ Faculty of Physics, Vilnius University, Vilnius, Lithuania, associated to ²⁰
- ⁸¹ Van Swinderen Institute, University of Groningen, Groningen, The Netherlands, associated to ³⁸
- ⁸² Universiteit Maastricht, Maastricht, The Netherlands, associated to ³⁸
- ⁸³ Tadeusz Kosciuszko Cracow University of Technology, Cracow, Poland, associated to ⁴¹
- ⁸⁴ Universidade da Coruña, A Coruña, Spain, associated to ⁴⁶
- ⁸⁵ Department of Physics and Astronomy, Uppsala University, Uppsala, Sweden, associated to ⁶⁰
- ⁸⁶ Faculty of Physics, Taras Schevchenko University of Kyiv, Kyiv, Ukraine, associated to ¹⁴
- ⁸⁷ University of Michigan, Ann Arbor, MI, USA, associated to ⁶⁹
- ⁸⁸ Ohio State University, Columbus, USA, associated to ⁶⁸

^a Universidade Estadual de Campinas (UNICAMP), Campinas, Brazil

^b Centro Federal de Educação Tecnológica Celso Suckow da Fonseca, Rio De Janeiro, Brazil

^c Department of Physics and Astronomy, University of Victoria, Victoria, Canada

^d Center for High Energy Physics, Tsinghua University, Beijing, China

^e Hangzhou Institute for Advanced Study, UCAS, Hangzhou, China

^f LIP6, Sorbonne Université, Paris, France

^g Lamarr Institute for Machine Learning and Artificial Intelligence, Dortmund, Germany

^h Universidad Nacional Autónoma de Honduras, Tegucigalpa, Honduras

ⁱ Università di Bari, Bari, Italy

^j Università di Bergamo, Bergamo, Italy

^k Università di Bologna, Bologna, Italy

^l Università di Cagliari, Cagliari, Italy

^m Università di Ferrara, Ferrara, Italy

ⁿ Università di Genova, Genoa, Italy

^o Università degli Studi di Milano, Milan, Italy

^p Università degli Studi di Milano-Bicocca, Milan, Italy

^q Università di Modena e Reggio Emilia, Modena, Italy

^r Università di Padova, Padua, Italy

^s Università di Perugia, Perugia, Italy

^t Scuola Normale Superiore, Pisa, Italy

^u Università di Pisa, Pisa, Italy

^v Università della Basilicata, Potenza, Italy

^w Università di Roma Tor Vergata, Rome, Italy

^x Università di Siena, Siena, Italy

^y Università di Urbino, Urbino, Italy

^z Universidad de Ingeniería y Tecnología (UTEC), Lima, Peru

^{aa} Universidad de Alcalá, Alcalá de Henares, Spain

*Deceased